

Intercomparison of tropical Indian Ocean circulation in ocean reanalysis and evaluation in CMIP6 climate models

Bhanu Deepika P^{1,2}, Soumya Mohan^{1,2*}, G. Srinivas^{1,2}

¹CSIR-National Institute of Oceanography, Dona Paula, Goa, India

²Academy of Scientific and Innovative Research (AcSIR), Ghaziabad, India

Correspondence :Soumya S Mohan,Physical Oceanography Division

E-mail: soumyamohan866@gmail.com

Abstract

In the present study, we assess the Tropical Indian Ocean (TIO) circulation features from the available ocean reanalysis products and climate models in the latest version of Coupled Model Intercomparison Project (CMIP6). We considered the following reanalysis products; Ocean Reanalysis System 5 (ORAS5), Estimating the Circulation and Climate of the Ocean (ECCO), Global Ocean Data Assimilation System (GODAS), Ensemble Coupled Data Assimilation (ECDA), the Bluelink Reanalysis (BRAN) and Simple Ocean Data Assimilation (SODA), and compared them against in-situ observations and the satellite-derived Ocean Surface Current Analyses Real-time (OSCAR). The reanalysis products underestimate the strength and location of the Wyrтки Jets. The BRAN reanalysis performed well compared to the other products in representing the TIO surface zonal currents, followed by ORAS5. The vertical extension of subsurface zonal currents in the equatorial Indian Ocean and their seasonal maxima are well captured in ORAS5. Thus, our analysis suggests that the ORAS5 is a qualitative product to estimate the TIO circulation. We further evaluated the TIO current patterns simulated by CMIP6 models with in-situ data/ ORAS5. The majority of the models show discrepancies in simulating equatorial and south equatorial current systems with a mean bias of 0.1cms^{-1} and 0.2cms^{-1} , respectively. NorESM2-MM, NorESM2-LM, CanESM5, CESM2-WACCM-FV2, and E3SM-1-ECA models showed a superior skill in reproducing the TIO circulation compared to the rest of the models. Our analysis highlights the importance of assessing various reanalysis products and coupled climate models in representing the circulation of the TIO and, consequently, their role in depicting regional weather and climate.

Keywords: Ocean currents, reanalysis, Wyrтки jets, south equatorial current, CMIP6 models

1. Introduction

Monitoring changes in ocean surface currents is critical for climate change studies as they are key heat and salt transporters. The major surface current systems of the Indian Ocean consist of monsoon currents, Wyrki jets (WJs), South Equatorial Counter Current (SECC), South Equatorial Current (SEC), and south Indian Ocean counter current (Schott et al., 2009; Phillips et al., 2021). The near-surface circulation north of 10°S is dominated by seasonally reversing monsoon currents (Schott 1983, Schott and McCreary 2001). The monsoon currents flow eastward during the summer monsoon and westward during winter monsoon (Shankar et al. 2002). The winter monsoon currents are commonly known as North equatorial currents (NEC) and which is replaced by southwest monsoon currents during summer. Other important seasonally reversing currents include Somali currents, equatorial currents, East India coastal current, and West India coastal current. The WJs are direct wind-forced inter-monsoon zonal surface currents along the equatorial Indian Ocean (Wyrki 1973). They play a significant role in the zonal distribution of upper ocean mass, heat, and salt across the equatorial Indian Ocean. The equatorial undercurrent (EUC) is often present below the equator during the seasons when winds have an easterly component (Reppin et al. 1999).

The upper South Indian Ocean is characterized by westward flowing SEC and boundary currents (Schott and McCreary, 2001). The SEC splits into Northeast and Southeast Madagascar currents near 17°S and the former feeds the East African coastal current and eventually crosses the equator into the north Indian Ocean during the southwest monsoon (McCreary and Kundu, 1988, Schott et al. 2009). The TIO circulation acts as a vital pathway for oceanic communication with the rest of the world's oceans (Schmitz, 1995). The low latitude inter-oceanic pathway, Indonesian Throughflow (ITF), for example, connects the tropical Pacific and Indian Oceans, whereas the Agulhas Leakage (AL) connects the Indian and Atlantic Oceans. The westward South Equatorial current is partially fed by ITF and Pacific water into the interior Indian Ocean (Sprintall et al. 2014, Chen et al. 2020). Along the southeast coast of Africa, a strong western boundary current regime known as the Agulhas Current regulates the outflow of the Indian Ocean into the Atlantic Ocean. The southern branch of SEC joins the Agulhas Current near the southern tip of Madagascar and contributes to the water exchange between the SIO and the Atlantic Ocean (Quartly et al. 2006). The part of the Agulhas water that does not curl back and that passes into the South Atlantic is known as Agulhas leakage (Gordon 2001). The inter-ocean exchange between the Indian and Atlantic Oceans majorly takes place through the Agulhas leakage pathway (Beal et al. 2011).

The studies on circulation variability at regional or global scale are constrained by geographical and temporal resolution of observations. The consecutive generations of the state-of-the-art climate

models participating in the CMIP have recently made significant advancements in simulating ocean circulation, by delivering sufficient samples for investigating ocean circulation and climate variability. Most of the models in CMIP6 experiments are upgraded versions of the models that participated in the previous phases. Compared to the previous versions, these models have a better representation of earth system processes, improved resolution, and physical parameterizations (Eyring et al. 2016). The climate models are to be evaluated comprehensively as they have developed primarily for projecting future climate. The representation of Indian Ocean circulation in various reanalysis products and the latest generation of climate models are not extensively evaluated. Recently, Zhang and Wang (2023) evaluated the zonal current structure of EUC and SEC in the Indian Ocean simulated by 29 climate models. However, their study is limited to selected zonal and meridional sections of the TIO. Recently, Lin et al. (2023) examined the simulations of equatorial ocean currents simulated by CMIP6 models in the Pacific Ocean and explored their substantial influences on the systematic bias of westward-extended sea surface temperature anomalies pattern during El Nino. Li et al. (2023) assessed the performance of CMIP6 models in representing various features of Equatorial undercurrent (EUC) in the Indian Ocean and compared them with CMIP5 models. However, a model-by-model evaluation of the surface circulation pattern of the Indian Ocean has not been done previously. Assessment of individual models in representing the climatological mean state is an important step towards reliable regional climate projections as they show different levels of skill in simulating specific climate variables over any ocean basin.

Reanalysis and satellite-based products are commonly utilized as proxies for direct observations when assessing basin-scale processes simulated by climate models due to their extensive spatial and temporal coverage over long periods. In situ observations undeniably stand out as the most valuable benchmark for assessing the accuracy of reanalysis products and model outputs. Nevertheless, they are constrained by notably limited spatial coverage and insufficient temporal continuity, presenting practical challenges for the Indian Ocean region. The ocean currents simulated by ocean reanalysis systems from various agencies differ substantially, as they use different ocean general circulation models (OGCMs) and data assimilation schemes to provide accurate estimates of the ocean states. Carton et al. (2019) intercompared and quantified discrepancies in ORAS5, ECCOv4r3, and SODA3 in representing temperature and salinity in various ocean basins. The global average surface warming and deep ocean warming trends exhibit considerable differences, despite the similarity in spatial patterns. The rate of warming is most pronounced in ORAS5, while ECCOv4r3 exhibits the weakest warming trend, especially for the Indian Ocean. Their study highlights the importance to

intercompare various reanalysis products to improve the accuracy of numerical models used and also to identify future directions for improvements in data assimilation.

Karmakar et al. (2018) evaluated various reanalysis products for the TIO region and discussed the diversity in the simulation of various parameters in them. They have analysed only four datasets such as GODAS, ECDA, ORAS4 and SODA, and the notable missing product from their assessment is BRAN2020, which was developed as a part of the Bluelink project in Australia (Oke et al. 2013; Chamberlain et al., 2021). They concluded that the ORAS4 product exhibits higher skill compared to other products in simulating surface circulation, SST and sea surface salinity. Additionally, we assess and compare various circulation features in ECCO, BRAN, the upgraded version of ORAS4 (ORAS5), along with previously assessed GODAS, SODA, and ECDA. Many recent studies have evaluated CMIP6 models in representing the mean state of SST, Mixed layer, heat fluxes, and equatorial current systems (e.g., Feng et al., 2023, Zhang and Wang 2023, McKenna et al. 2024). However, the mean state of the TIO specifically focusing on major circulation features and assessment of various CMIP6 models has not been explored in previous researches. In the present study, we evaluate and intercompare various features of ocean currents in six reanalysis products and 45 climate models participating in CMIP6. The rest of this paper is organized as follows: Section 2 describes the datasets used and methods followed. The main findings of the study are documented in section 3. The results are summarized in section 4.

2. Data and methods

2.1 Observational data

In the present study, we use OSCAR currents derived from satellite measurements to intercompare and evaluate the near-surface circulation in various reanalysis datasets and CMIP6 models. The OSCAR surface currents are constructed by compiling various satellite and observation data sets including sea surface heights, scatterometer winds, and both advanced very high-resolution radiometer and in situ sea surface temperatures using a simplified physical model for ocean mixed layer (Bonjean and Lagerloef 2002, ESR 2022). The horizontal velocity field comprises a blend of geostrophic, Ekman–Stommel, and thermal-wind currents. These approximations are invalid near the equator and to address this challenge, a weak formulation of the momentum equations is solved using a set of 12 orthogonal polynomials to approximate the velocity solution as a function of latitude between 8°N and 8°S. The equatorial solutions are joined to the classical momentum balance formulations poleward of 8° using a linear taper function between 5° and 8° latitude (Lagerloef et al. 1999, Bonjean and Lagerloef 2002). The OSCAR currents depict the mean flow of currents across a surface layer with a thickness of 30

meters (Johnson et al. 2007, Bonjean and Lagerloef 2002). Previous studies have shown that the OSCAR current product is skillful in simulating surface current systems of the Indian Ocean (Sikhakolli et al. 2013, Rahaman et al. 2018 etc.,). The efficacy of various products in representing the mean state of upper ocean currents is validated using the current measurements obtained from four acoustic Doppler current profiler (ADCP) mooring locations (Table 1) of the Research Moored Array for African-Asian-Australian Monsoon Analysis and Prediction (RAMA; McPhaden et al. 2009). The data availability at depth ranges offered by RAMA mooring data are based on upward-facing Acoustic Doppler Current Profilers (ADCP), ranging from 30 m to about 335 m at intervals of 5 m. The uncertainties associated with RAMA buoy data primarily revolve around factors such as measurement errors, instrument calibration, data transmission issues, environmental disturbances affecting floating buoy stability, and large data gaps (McCarty et al. 1997). The current velocities recorded by RAMA ADCP moorings closely align with point velocity measurements, with discrepancies typically falling within a range of 5 cm/s (source: <https://www.pmel.noaa.gov/gtmba/data-quality-control>).

2.2 Reanalysis datasets

The zonal and meridional currents are extracted from the following reanalysis products are considered in the study: The simple ocean data assimilation (SODA) version 3, global ocean data assimilation system (GODAS) version 2, The ECMWF ocean reanalysis system (ORAS5) version 5, Estimating the circulation and climate of the ocean (ECCO) version 4, ensemble coupled data assimilation (ECDA) version 3.1, and the blueslink reanalysis (BRAN2020) product. Details of these products are given in Table 2 and in the following subsections.

a. Global Ocean Data Assimilation System (GODAS)

The operational GODAS was built on the earlier version of the ODAS configured for the Pacific Ocean (Ji et al., 1995; Behringer et al., 1998). The GODAS assimilates observations using version 3 of the Geophysical Fluid Dynamics Laboratory (GFDL) Modular Ocean Model (MOM3) and a three-dimensional variational (3DVAR) assimilation scheme (Derber and Rosati et al. 1989). As forcing, it employs momentum flux, heat flux, and freshwater flux from the National Centre for Environmental Prediction (NCEP) atmospheric reanalysis version 2. In GODAS, SST is the adjusted Reynolds SST (Reynolds et al. 2002) with a relaxation time scale of 5 days and the sea surface salinity is adjusted to Levitus monthly climatological fields (Levitus et al. 1994), with a relaxation time scale of 10 days. Subsurface temperature from expendable bathythermographs (XBTs), the tropical atmosphere-ocean (TAO) array of moored buoys, as well as Argo and similar floats, were utilized for assimilation. The currently available GODAS versions assimilates synthetic salinity profiles constructed using the local

T-S relationship of the Levitus's climatology into the ocean model (Behringer and Xu 2004; Saha et al. 2006). The altimetry sea level and Argo salinity datasets have not been assimilated into GODAS and are scheduled for inclusion in future versions. The horizontal resolution is 1° , with a meridional resolution of $1/3^\circ$ within 10° of the equator. It contains 40 vertical levels ranging from 5 m to 4478 m, with data availability from 1980 to the present.

b. Ocean Reanalysis System (ORAS5)

The Ocean ReAnalysis System 5 (ORAS5) uses the fifth generation of ocean reanalysis system at the European Centre for Medium Range Weather Forecast (ECMWF) and which uses Nucleus for European Modelling of the Ocean (NEMO) model version 3.4 as the ocean model. Compared to 1° horizontal resolution and 42 layers in ORAS4, the ocean model resolution has been increased to an eddy-permitting resolution of 0.25° in the horizontal and 75 vertical levels in ORAS5 (Zuo et al., 2019). Forcing fields for ORAS5 are derived from the atmospheric reanalysis ERA-Interim and ECMWF operational Numerical Weather Prediction which uses a Coordinated Ocean-Ice Reference Experiment (CORE) data assimilation system to include the impact of surface waves on the exchange of momentum and turbulent kinetic energy (Large and Yeager, 2009). In addition, the global mean sea level trends and thermohaline fields are used to modify the surface fluxes of heat and freshwater (Zuo et al. 2019). The updated NEMOVAR data assimilation scheme with a new Rossby-radius-dependent spatial correlation length-scale has been employed in ORAS5 (Zuo et al., 2015, Zuo et al., 2017).

c. Estimating the Circulation and Climate of the Ocean (ECCO)

The ECCO project intends to combine accessible global ocean and sea-ice data with a state-of-the-art ocean general circulation model with eddy-permitting resolution. The least-squares fit of a global full-depth-ocean and sea-ice configuration of the Massachusetts Institute of Technology general circulation model (MITgcm; Marshall et al., 1997) assimilated with available satellite and in-situ data using the Green's function method (Menemenlis et al., 2005). The air-sea heat fluxes and vertical mixing coefficients are directly assimilated using variational data assimilation scheme (Forget and Ponte 2015). Atmospheric forcing fields are derived from ERA-Interim, and applies correction to the surface fluxes. Unlike the previous versions, ECCO v4 uses a nonlinear free surface formulation and real freshwater flux boundary condition to simulate sea level (Fukumori et al. 2007). The model consists of 50 vertical layers, with vertical resolution ranging from 10 m at the surface to 456 m at the bottom and with a horizontal resolution of $1^\circ \times (0.4^\circ - 1^\circ)$.

d. Ensemble Coupled Data Assimilation (ECDA)

The GFDL-ECDA system is made up of an ensemble-based filtering algorithm applied to a climate model (Delworth et al. 2006) from GFDL. The oceanic component of ECDA is MOM4 and is configured with $1^\circ \times 1^\circ$ horizontal resolution telescoping to $1/3^\circ$ meridional spacing near the equator and 50 vertical levels. The assimilation scheme is based on the probability distribution estimates of the observed climate states. It uses a two-step data assimilation algorithm for local and impacted grid points. The system has assimilated observed surface and subsurface temperature and salinity whereas the atmospheric parameters are based on NCEP reanalysis. The primary purpose of the ECDA project is to develop a state-of-the-art data assimilation system that incorporates near-real-time data and can produce high-quality ocean state products. The current study makes use of ECDA currents from version 3.1.

e. Simple Ocean Data Assimilation (SODA)

SODA version 3.3.1 uses GFDL MOM5 as ocean component with fully interactive sea ice and improved horizontal resolution of 0.25° and 50 vertical levels (Carton et al., 2018). The surface forcing of SODA v3.3.1 is based on radiative heat fluxes and near-surface atmospheric variables from ERA-Interim and assimilates only the basic hydrographic dataset and SST. SODA 3.3.1 does not assimilate altimeter data and it utilizes CTD and XBT hydrographic profiles from the WOD13 (Boyer et al. 2013) and AVHRR SST (Casey et al., 2010). The forcing variables are applied to the ocean–sea ice system through the GFDL Flexible Model System flux coupler, which includes the Coupled Ocean–Atmosphere Response Experiment (Fairall et al., 2003) version 4 (COARE4) bulk formulas.

f. The Bluelink ReANalysis (BRAN)

The Bluelink ReANalysis version 2020 (BRAN2020; Chamberlain et al. 2021a,b) is developed as a part of the Bluelink project, under the partnership between the Commonwealth Scientific and Industrial Research Organization (CSIRO), the Bureau of Meteorology (BoM), and the department of defence. The model configuration of BRAN2020 uses Ocean Forecasting Australian Model version 3 (OFAM3; Oke et al. 2013) and it is configured with MOM version 5 as the ocean component. OFAM3 has a horizontal resolution of 0.1° horizontal grid resolution between 75°S and 75°N , with 5m vertical resolution to 40m depth and 10° vertical resolution to 200m depth. Surface heat fluxes, momentum flux and fresh water flux from the latest version of Japanese Reanalysis (JRA-55) are used to force OFAM3. BRAN assimilates in situ, reanalysis, and satellite data using the Ensemble Optimal Interpolation data assimilation system implemented with a novel multiscale approach to constrain the broad-scale ocean properties and the mesoscale circulation through a two-step process (Sakov et al.

2014). Observations of temperature and salinity profile are assimilated from the Copernicus Marine Environment Monitoring Service (CMEMS), Coriolis Ocean dataset for ReAnalysis (CORA v5 & v5.1; Cabanes et al. 2013) and from a near-real time database of Australia Bureau of Meteorology. It also assimilated along-track SST and SLA data from the Along-Track Scanning Radiometer and Radar Altimeter Database system. Most aspects of the circulation simulated by BRAN versions are realistic and is suitable for broader analysis to better understand the upper ocean dynamics at mid and low latitudes (Oke et al. 2013).

2.3 CMIP6 Models

The historical simulations of zonal and meridional currents from 45 CMIP6 models are used in the study. The selection criterion for the models was based on the availability of monthly u and v currents data for the r1i1p1f1 (where "r" stands for realization, "i" for initialization, "p" for physics, and "f" for forcing) ensemble variant in the historical simulations at the time of conducting the data analysis. A list of CMIP6 models considered in the present study, details of their development agencies, and the horizontal resolutions are given in Table 3. The ocean vertical coordinate system of the climate models is typically the traditional z height levels (or the rescaled height z^*), but some models use isopycnal, sigma or hybrid coordinates. Although the historical experiment runs of these models cover the period 1850-2014, in this work, we consider the simulations for the period 1993-2014 to comply with the OSCAR product for the evaluation.

2.4 Methodology

The study evaluates zonal and meridional currents extracted from six reanalysis products described in the previous sections for the TIO region with reference to the satellite and in situ products for the selected locations. The climatology of surface circulation from reanalysis products is compared against reference datasets (OSCAR, and RAMA moorings) during the period 1993-2017. Here, we have estimated the bias as the difference between the reanalysis products/models and the reference data (for e.g., BRAN – OSCAR). The OSCAR currents represent the mean flow of currents across a surface layer with a thickness of 30 meters. To be consistent with the OSCAR currents, the zonal and meridional components of currents extracted from reanalysis and CMIP6 models are averaged for the upper 30 meters to evaluate the mean state. All the gridded reanalysis products and CMIP6 models have interpolated onto a uniform $1^\circ \times 1^\circ$ grid from their native horizontal resolution using a bilinear interpolation method. This facilitates validation with observations and enables intercomparison among them. The statistical methods such as the root mean square error (RMSE; Chai et al. 2014) and the

pattern correlation coefficient (PCC; Taylor et al. 1990) were used to quantify the skill of reanalysis and CMIP6 models.

The PCC, representing the Pearson product-moment coefficient of linear correlation, assesses the correlation between the values of same variables at corresponding locations on two separate spatial maps. It can be calculated as:

$$\text{PCC} = \frac{\sum_{i=1}^N (x_i - \bar{x})(y_i - \bar{y})}{\sqrt{\sum_{i=1}^N (x_i - \bar{x})^2} \sqrt{\sum_{i=1}^N (y_i - \bar{y})^2}},$$

where x represents the modeled value and y represents the observed value, with N being the number of samples.

The RMSE measures the extent of the deviation of the model values from the observed values, and its calculation is as follows:

$$\text{RMSE} = \sqrt{\frac{\sum_{i=1}^N (x_i - y_i)^2}{N}}$$

The PCC and RMSE are frequently employed together to evaluate a model's predictive skill as they effectively quantify the relationships between modelled and observed values. A dataset is considered to be highly skilful, when the RMSE and PCC values are close to 0 and 1, respectively.

In the present study, currents from four RAMA buoy locations were considered due to the limited and non-consistent availability at the temporal scale of surface current data in other RAMA sites in the Indian Ocean. The evaluation of reanalysis products and CMIP6 models with reference to RAMA buoys involves considering concurrent periods of availability from them. To evaluate reanalysis products and CMIP6 models, we have extracted currents at the buoy locations from reanalysis products and CMIP6 models. A similar approach has been employed in previous studies on climate model evaluation (e.g., Krishnan and Bhaskaran 2020, Bhattacharya et al. 2022).

The zonal volume transport of the Indian Ocean with the Pacific and Atlantic Oceans can be estimated using the equation,

$$V_h = w_{NS} \int_{-D}^0 u dz,$$

where w_{NS} is the North-South distance of the channel and the zonal velocity (u) is integrated from $z = -D$ to $z = 0$.

Following Makarim et al. (2019), we consider a meridional section at 115.5°E and 10.5-15.5°S to estimate the Indonesian Through Flow (ITF) volume transport (Figure S1). The zonal current along this section for the depth range of 0-700m is integrated to obtain the volume transport and the westward transport (towards the Indian Ocean) is defined as negative. The transport computed across this section integrates the zonal flow coming into the Indian Ocean through the Lombok Strait, Ombai Strait, and Timor Passage which are the three major exit pathways of ITF to the Indian Ocean (Sprintall et al. 2009). The Agulhas leakage (AL) is estimated along a meridional section at 26.5°E, and 34.5–36.5°S as shown in Figure S1 (Makarim et al. 2019).

3. Results and discussions

3.1 Representation of TIO surface circulation in ocean reanalysis and CMIP6 models

In this section, we first evaluate the climatological features in the different reanalysis products and 45 individual CMIP6 models compared to the OSCAR product. The annual mean climatology of surface circulation from OSCAR and reanalysis products are shown in Figure 1. The OSCAR currents display strong eastward currents of magnitude 0.25 ms^{-1} between the equator and 5°S and a strong western boundary current system such as Somalia and Oman currents with a magnitude 0.2 ms^{-1} is observed in the north Indian Ocean. Annually, the equatorial surface currents are eastward due to the dominance of semi-annual WJs during the transition months (Wyrki 1973). The reanalysis products reveal diverse distribution in representing the equatorial current system. The strong westward SEC between 7°- 20°S is observed in OSCAR and all the reanalysis products, but the southward extension slightly differs from product to product. All the products except ECDA feature a strong anticyclonic gyre in the Arabian Sea and Bay of Bengal (Figure 1e).

Although the OSCAR product is skillful in simulating surface current systems of the Indian Ocean, large bias and RMSE of surface currents are reported for the equatorial region (e.g., Sikhakolli et al. 2013; Rahaman et al. 2019; Johnson et al. 2007). Comparison of OSCAR currents with collocated RAMA buoy observations over the Indian Ocean showed RMSE values of 16.6 cm/s for zonal current and 13.3 cm/s for meridional current (Rahaman et al. 2018). It is to be noted that all the reanalysis products underestimate the eastward equatorial currents in the Indian Ocean (Figure 2). The magnitude of eastward equatorial current bias is less in ECCO, whereas it largely overestimates zonal currents over the southwestern Indian Ocean (Figure 2c). GODAS exhibits strong underestimations of equatorial currents, evidenced by pronounced westward currents north of the equator and significant

eastward biases in zonal currents south of the equator (Figure 2a). ECDA has large bias in simulating equatorial currents and underestimation of 0.09m/s is observed with reference to OSCAR. Johnson et al. (2007) and Sikhakolli et al. (2013) assessed the skill of OSCAR currents using in situ observations in the tropical Pacific and Indian Ocean. Their investigations highlighted discrepancies in OSCAR's performance, particularly in the equatorial regions. They found that the root mean squared difference ranged from 14 to 23 cm/s in the equatorial Pacific and ~ 30 cm/s in the equatorial Indian Ocean. Previous studies have attributed the mismatch between the OSCAR currents and in situ currents measurements over the equatorial regions to the errors in local acceleration terms in the algorithm used for calculating OSCAR currents (Johnson et al. 2007, Mcgregot et al. 2016). Rahaman et al. (2019) suggested that the significant bias of GODAS compared to OSCAR in representing the equatorial current is due to inaccuracies associated with the OSCAR dataset. The discrepancies observed in various reanalysis products in representing the equatorial currents may be partially attributed to the inaccuracies associated with the modified geostrophic and Ekman theories involved in the computation of OSCAR currents.

Previous research has reported that ECMWF ORAS4 and ORAS5 currents are most skillful in reproducing various circulation features in the north Indian Ocean (e.g., Karmakar et al. 2018, Chu et al. 2022). Figure 3 shows that BRAN is most skillful in representing the surface circulation of TIO, followed by ORAS5 and ECCO as they characterize higher values of PCCs and lower RMSE values. The improved simulation of surface circulation in BRAN is attributed to the greater number of observations, along track observations of SLA, SST, and advanced multiscale data assimilation approach (Chamberlain et al. 2021a). The spatial resolution of BRAN is 0.1° , which is the finest among all the reanalysis datasets considered in the study (Table 3). The PCCs between the annual climatology of zonal currents in BRAN and ORAS5 with OSCAR are 0.75 and 0.55, respectively. The RMSE values in them are 0.12ms^{-1} and 0.14ms^{-1} , respectively. The GODAS product has the smallest PCC and highest RMSE of 0.35 and 0.17m/s , respectively, for representing the annual climatology zonal currents over the TIO for the period 1993-2017. Surface circulation bias during the summer season in various reanalyses is the same as shown for the annual climatology, whereas the winter currents are better represented in them (figure not shown). GODAS is shown to have a large eastward current bias in the south TIO. GODAS, ECCO and ECDA display large biases in the southwestern IO region compared to the rest of the products. Karmakar et al. (2018) assessed four reanalysis products, namely GODAS, ECDA, ORAS4, and SODA, revealing that ORAS4 exhibits a realistic representation of surface circulation compared to the other reanalyses. However, it's worth noting that its upgraded version ORAS5 comprises enhanced horizontal and vertical resolution, improved parameterizations,

additional perturbations in forcings, an ensemble approach bias correction technique, and assimilation of a greater number of observations when compared to its predecessor, ORAS4. The present study highlights the superior skill of the BRAN reanalysis product in representing the mean state of surface zonal currents over ORAS5. We also evaluated ECCO, which is another notable missing product in their study and our study shows that ECCO is also skilful for TIO surface circulation followed by BRAN, and ORAS5.

The climatological zonal currents over the equator are characterized by weak (strong) westward currents during the summer (winter) monsoon season (McPhaden et al. 2015). It can be seen from Figure 4 that the eastward currents during inter-monsoon seasons exist throughout the zonal extent of the equator in all the reanalysis and OSCAR products. However, the eastward extension and magnitude of westward currents have large deviations in various datasets. The strong eastward currents of the equatorial Indian Ocean, called the Wyrтки jets are forced by the inter-monsoon equatorial westerlies (Wyrтки, 1973). They are identified during the spring and fall seasons and have distinct characteristics including their magnitude and flow pathways (Han et al. 1999, Zheng et al. 2012). The mean seasonal cycle of the zonal velocity over the Wyrтки Jet location ($50^{\circ} - 90^{\circ}\text{E}$; $2^{\circ}\text{S} - 2^{\circ}\text{N}$) and time series of spring and fall jets are shown in Figure S2. Previous studies (e.g., McPhaden et al. 2015, Duan et al., 2016, Joseph et al., 2012) have utilized OSCAR zonal currents to examine the variabilities associated with Wyrтки Jets. Recently, Huang et al. (2023) utilized OSCAR product to understand the latitudinal structure of WJs, monsoon currents, and SECC along 80.5°E at seasonal to interannual timescales. In May, the spring WJs reaches its peak and is slightly weaker (up to 0.25 ms^{-1}) and does not last as long as its fall counterpart (Figure S2b, c). The fall WJ reaches its maximum in November ($> 0.3 \text{ ms}^{-1}$), according to the OSCAR dataset (Figure S2a). The seasonal climatology of WJs in ECDA has a large overestimation (0.6 ms^{-1}) during the summer monsoon (June-September) due to the stronger westward currents compared to other data products (Figure S2a). BRAN product is shown to have the highest skill in representing the spring and fall surface climatology of WJs as shown by the highest PCCs (Table 4). Despite the large biases in the magnitude of the time series in ECDA and GODAS, all the reanalysis products are able to capture the seasonal climatology during spring and fall reasonably well. Figure S2 show that BRAN, ORAS5, and ECCO products have less year-to-year magnitude difference with reference to the OSCAR-derived spring and fall jets.

Many recent studies have reported simulation skills of state-of-the-art climate models in representing various air-sea parameters over the TIO (e.g., Bhattacharya et al. 2022; Sajidh and Chatterjee 2023), but a model-by-model evaluation of surface circulation of TIO has not been documented before. In the present study, we assess the surface circulation in 45 climate models with

reference to OSCAR currents and the vertical structure of the upper ocean at selected locations corresponding to in-situ buoy observations using observations and ORAS5 reanalysis product. To be consistent with the OSCAR currents, the zonal and meridional components of currents extracted from CMIP6 models are averaged over the upper 30 meters to evaluate the mean state. The major upgrades in CMIP6 models compared to its earlier versions are in terms of their horizontal and vertical resolutions in the atmosphere and ocean components, improved model physics and dynamic core (McKenna et al., 2020). For example, the horizontal resolution of the GFDL-CM3 model ($0.9^{\circ}\times 1^{\circ}$) with 50 levels has been improved to $0.25^{\circ}\times 0.25^{\circ}$ horizontal resolution and 75 vertical levels in its CMIP6 version GFDL-CM4. We evaluate the surface currents in 45 CMIP6 models for the period 1993- 2014 (Table 3), for their consistency with the OSCAR product. Figure 5 shows the inter-model diversity in the representation of the climatological mean state of surface circulation in various CMIP6 models. Most of the models and their multi-model mean (MMM) are in good agreement for representing the surface circulation with OSCAR product. However, the models display large discrepancies in simulating equatorial currents and strength of the surface SEC system (Figure 5). Only few models including IPSL-CM6A-LR, IPSL-CM6A-LR-INCA, and MPI-ESM-1-2-HAM overestimate the eastward current in the equatorial Indian Ocean. MCM-UA-1-0 shows strong underestimation in representing eastward zonal currents in the TIO. The southern Indian Ocean circulation exhibits notable disparities across the majority of models, notably in BCC-ESM1, FGOALS-f3-L, FGOALS-g3-L, MCM-UA-1-0, and NESM2. The westward SEC is represented in all the models but its magnitude and southward extension vary in individual models. For instance, while MPI-ESM models display southward expansion of the surface SEC, the CESM2 models show the core velocity of SEC predominantly centered north of 15° S. The surface circulation of the north Indian Ocean is simulated reasonably well in these models.

We depicted the mean-state biases of CMIP6 models along with their MMM in representing the TIO surface circulation against the satellite currents shown in Figure 6. The MMM displays notable biases over the equatorial Indian Ocean, and 40 out of 45 models underestimate the eastward equatorial zonal currents. Previously Liu et al. (2016) documented the diversity of CMIP5 models in representing the spring and fall Wyrтки Jets. They showed that most of the models simulate the WJs by a delay of one month due to the late onset of westerly winds. Previous studies linked the zonal current biases of CMIP6 models to surface wind forcing (Zhang and Wang 2023, McKenna et al. 2024). Models including CanESM5, CAS-ESM2-0, IPSL-CM6A-LR, and NorESM2 models shown to have less bias in representing surface circulation over the equatorial Indian Ocean. Large underestimation of equatorial currents is found in models from BCC-ESM1, CAMS-CSM1-0, CMCC-CM2-HR4, EC-

EARTH3 models, GISS models except GISS-E2-2-H, MCM-UA-1-0, MIROC6, and NESM3. However, these models represent the surface circulation over the north Indian Ocean reasonably well. Over the south Indian Ocean region, models have differences in performance especially in simulating the SEC system. Both the FGOALS-f3-L and FGOALS-g3 models largely underestimate SEC as shown by strong eastward counter currents between the 10°-20°S zonal band. Whereas all four CESM models overestimate the westward SEC system and the surface circulation in them characterizes strong southwestward currents over the south TIO region. The eastward equatorial currents are overestimated in MPI-ESM-1-2-HAM, MPI-ESM-1-2-HR and MPI-ESM1-2-LR models, unlike the majority of CMIP6 models. Their CMIP5 version, MPI-ESM-LR also reported having a large magnitude of equatorial currents, especially during the boreal fall season (Liu et al. 2016). The majority of the models show discrepancies in simulating equatorial and south equatorial current systems with a mean bias of 0.1cms⁻¹ and 0.2cms⁻¹, respectively. It is interesting to see that some of the models from the same centre show basin-wide common biases. For e.g., five EC-Earth3 models of EC-Earth Consortium, Europe characterize identical biases and the same can be observed in CESM2 models developed by NCAR, USA. Sharing of earth system components and common parameterization schemes between models from the same or different centers are one of the reasons for common biases reported in CMIP5 and CMIP6 models (Knutti et al. 2010; 2013, Seland et al. 2020). In contrast, significant bias differences can be observed in individual models from same agency, for e.g., models from Beijing Climate Center (BCC), China and NASA Goddard Institute for Space Studies (NASA GISS), USA (Figure 6).

To further verify the skill of models, we use statistical methods PCC and RMSE for each model shown as in Figure 7. A model is listed to be skilful for simulating the climatological mean state of a specific climate variable when it has a higher PCC and negligible RMSE value (Mishra et al. 2018). The annual mean climatology of surface zonal currents in all the models except FGOALS-f3-L and FGOALS-g3-L show statistically significant PCC at 95% confidence level against the same in OSCAR. Only 9 out of 45 models have PCC above 0.75 and they have the lowest RMSE compared to OSCAR data. These models include NorESM2-MM, NorESM2-LM, MPI-ESM-1-2-LR, IPSL-CM6A-LR-INCA, IPSL-CM6A-LR, E3SM-1-1-ECA, E3SM-1-1, CESM2-WACCM-FV2, and CanESM5. Liu et al. (2016) showed that all the CESM1 models and NorESM1 models in the CMIP5 have higher PCC in representing the mean climatology of zonal currents over the equatorial Indian Ocean. Recently Bhattacharya et al. (2022) listed the models such as NorESM2-LM, CanESM5, CESM2-WACCM-FV2, CESM2, CESM2-WACCM, and IPSL-CM6A-LR are skilful in representing the SST variabilities over the TIO region. Based on the ratio of PCC to NRMSE, it is noted that the

NorESM2-MM is the best model, while FGOALS-g3 turns out to be the least skilful model in representing the climatological mean state of the surface circulation over the tropical Indian Ocean region. Recent researches have suggested that NorESM2-MM is skilful in simulating climatological mean state, interannual variability, and representation of boundary currents (Song et al. 2022, Held et al. 2019). We list out NorESM2-MM, NorESM2-LM, CanESM5, CESM2-WACCM-FV2, and E3SM-1-ECA as the highest skillful models as they characterize marginal bias and higher skill score compared to OSCAR.

The inter-model spread of PCC, calculated as the standard deviation of PCC values across 45 climate models, is found to be 0.15. However, this spread improves to 0.07 when we exclude both the FGOALS models, as their PCCs are not statistically significant. The RMSE value in 39 models exceed 0.1ms^{-1} and the higher values indicate the greater deviation of climatological mean state with reference to the observation-based product. Both the FGOALS models (FGOALS-f3-L and FGOALS-g3-L) are shown to have large deviation in magnitude relative to the observation as indicated by lowest PCC and highest RMSE values. It is worth noting that these models have poor vertical resolution compared to the remaining models (Table 4). However, skill of a model is not directly linked to horizontal and vertical resolution. For instance, the finest model considered in the study, GFDL-CM4 has a lower PCC value of 0.74 and a higher RMSE value of 0.11ms^{-1} and is ranked as 16th among the 46 models (Table 2, Figure 7c). The NorESM2-MM model has horizontal resolution of 1° and has only 53 vertical resolution. Chen et al. (2021) suggested that unlike the CMIP5 models, the dependency of model skill on horizontal resolution is less significant in CMIP6. Apart from the model resolution, the uncertainties in certain other factors such as errors in forcing variables, initial conditions, inaccurate physical parameterization etc. are crucial sources of biases in CMIP6 models. The ranking of the models has not altered majorly when we consider BRAN as the reference data (figure not shown).

Figures 5 and 6 show highlight the underestimation of equatorial surface circulation in CMIP6 models. Zhang and Wang (2023) simulated biases of zonal currents are linked to hydrography and wind forcing simulation biases. The weaker near-equatorial flow in CMIP6 models, in contrast to reanalysis data, is ascribed to surface wind biases (McKenna et al., 2024). These biases in equatorial surface winds are associated with inaccuracies in the Walker circulation and anomalous spatial extension of the equatorial Pacific cold tongue (Li et al. 2023). McKenna et al. (2024) have recently shown significant overestimations in Somali currents during boreal summer. The performance of coastal boundary currents in the northern Indian Ocean remains uncertain in our investigation since our study does not specifically target boundary currents using high-resolution climate models. These particular aspects will be subject to thorough examination in a forthcoming detailed study. The

atmospheric processes in particular surface winds are a primary cause of biases in Indian Ocean SST and surface circulation (Li et al. 2023, Zhang and Wang 2023). Reducing these biases would improve the simulation of climate variability in the Indian Ocean toward more reliable climate projections and predictions.

Natural variability like ENSO, IOD, PDO, SAM etc. are strong indicators of a climate model fidelity. Fasullo et al. (2020) noted a progressive improvement across various generations of CMIP models in their representation of both extratropical and tropical climate modes. However, they found that only a small subset of models demonstrate satisfactory skill in representing these climate modes in CMIP6. Hence, the 22-year climatological mean state of major circulation features of TIO in CMIP6 models discussed in this study is impacted by the phases of natural climate variability in a manner distinct from that observed in the observational record. Further research is needed to explore underlying physical dynamics behind the systematic model biases in representing Indian Ocean circulation and its link to intrinsic climate modes.

In summary, this section inferred the performance of individual reanalysis datasets and CMIP6 models and showed the discrepancies in them compared with OSCAR currents. Although uncertainties exist in the OSCAR data, the large-scale surface circulation features of TIO in them is consistent with various reanalysis products including BRAN, ORAS5, ECCO and SODA. Among all the reanalysis considered in the present study, BRAN, ORAS5, and ECCO products showed superior skill in capturing the surface circulation. The higher skill of BRAN, ORAS5, and ECCO in representing surface zonal currents may be attributed to assimilation of satellite SLAs (Table 2). The CMIP6 models largely underestimates the strength of equatorial currents and overestimates the SEC system. Nevertheless, it is crucial to understand the vertical structure in these products in comparison to observations, as equatorial currents play a significant role in redistributing heat and salt between the western and eastern Indian Ocean. The following section explores the vertical structure of ocean currents in the reanalysis products.

3.2 Evaluation of the upper ocean vertical structure in reanalysis and CMIP6 models

The representation of subsurface zonal currents in the upper layer in various reanalysis products is examined for selected locations of TIO where the in-situ ocean current observations are available from RAMA moorings. The evaluation of upper ocean circulation in reanalysis products against in situ observations is crucial to assess their reliability. Also, evaluating these products allows ocean modelers to identify and understand the region-specific biases, which is essential for minimizing errors when using them as boundary conditions in regional models. The mean seasonal cycle of the zonal velocity

in RAMA observations and reanalysis are constructed based on the available period for each location (Figure 8). Details of in-situ observations based on the RAMA currents mooring used for the inter-comparison are shown in Table 1. The three moorings are over the equatorial region and the comparison of upper ocean vertical profiles in reanalysis products with reference to in-situ observations can provide valuable insights into the performance of these products in capturing the dynamics of the equatorial Indian Ocean. The two strong eastward WJs can be observed in the equatorial moorings and the spring jets are deeper than the fall jets although the latter is climatologically stronger than the former. The vertical extension of the strong velocity core of spring WJs is found up to 180m in the equatorial moorings at 67°E, 80.5°E, and 90°E and the fall jets are confined to upper 130m along the equator. The semiannual WJs are well captured in all the reanalysis products but their vertical extension during both spring and fall seasons are different in various products. The magnitude and vertical distribution of spring WJs in the three locations are well simulated in BRAN whereas the fall jets are misrepresented in it compared to the in-situ observations. The fall jets in the three locations are better represented in ECCO and ORAS5, but the spring jets are not well captured in the former at 90°E.

The PCCs and RMSEs of upper ocean zonal currents extracted at RAMA buoy sites in reanalysis products are listed in Table 5. Highest PCC and lowest RMSE at 67°E is found in ECCO and the second highest skillful product is ORAS5. At 80.5°E, and 90°E ORAS5 characterises highest PCC and lowest RMSE values followed by ECCO. It can be seen from Figure 8 and Table 4 that the equatorial zonal current structure is better represented in ORAS5 and ECCO compared to other reanalysis products. It is to be noted that ORAS5 has the highest vertical resolution, and both ECCO and ORAS5 have the finest spatial resolution after BRAN (Table 2). Although BRAN is most skillful in representing surface circulation of TIO, the subsurface currents in the upper layers of equatorial region are not well simulated in it. Since the data availability at 106.75°E, 8.5°S is restricted to one annual cycle, we have not included zonal current structure at this location in Figure 8, but shown as Figure S3. It is worth noting that the seasonal cycle of subsurface zonal currents at 106.75°E, 8.5°S is most consistent with BRAN (Figure S3) and shows highest PCC of 0.81 and lowest RMSE of 0.12m/s (Table 5). The better skill of BRAN at this location may be attributed to the improved assimilations methods and greater number of observations in the south Indian Ocean such as in situ observations of temperature and salinity and measurements from Argo floats, surface drifting buoys, XBT, sea-mammal moorings, ship-borne surveys and underway systems (Chamberlain et al. 2021b). Recently Russo et al (2022) showed that BRAN outperforms other reanalyses in representing coastal SSTs along South Africa but it misrepresents the vertical structure of currents. This study has found that ORAS5,

BRAN, and ECCO are skilful for representing upper ocean circulation features of TIO among the commonly used reanalysis products.

The surface and subsurface currents in the upper 300m in CMIP6 models MMM are compared with observations from two RAMA buoy sites (Figure 9). We exclude the location 67°E as it doesn't have overlapping data availability with CMIP6 historical simulations. The seasonal cycle of zonal currents and its vertical extension is represented in the MMM for the two equatorial locations at 80.5°E and 90°E. The MMM underestimate the strength of subsurface core velocity of both spring and fall WJs (Figure 9). It is worth noting that the MMM well captures the vertical extension and depth at which core velocity of spring WJs located. However, the fall jets are largely underestimated and anomalously extended westward at 80.5°E (Figure 9a1&a2). In contrast, the spring jets show anomalous vertical extension at 90°E in MMM and fall jets are fairly well simulated (Figure 9b1&b2). The seasonal cycle during 2009 obtained from MMM at 106.75°E, 8.5°S is highly inconsistent with observation as it failed to simulate eastward zonal velocity and its vertical structure (Figure S4). The climatological seasonal cycle averaged at equator (45°E-100°E) for the period 1993-2014 in MMM is compared with ORAS5 (Figure 9c1&c2). The core of both spring and fall jets are located within 150m depth however, their vertical extension is unrealistic in MMM.

The inter-model scatter plot between PCC and RMSE in representing the vertical profile of the seasonal cycle also display the higher skill of NorESM2-MM, CESM2-WACCM-FV2, CanESM5, E3SM-1-ECA, MMM, etc., (Figure 9c2 & c3). The inverse relation of PCC and RMSE for simulating the seasonal cycle holds for the two RAMA buoy locations, with correlation coefficients found to be -0.7, and -0.73, respectively, for the two locations. The individual CMIP6 models are consistent in terms of both magnitude and shape of the seasonal cycle at various subsurface levels as shown by positive PCC values. The disparities observed between CMIP6 models and RAMA observations in representing the mean state of zonal currents can also be attributed to inadequately resolved local processes in coarse-resolution climate models. For instance, the unresolved ocean mesoscale processes not only affect the mean state but also have implications for climate variability and future climate responses (Hewitt et al., 2020). We also compare the vertical structure of equatorial currents (45°E-100°E; 2°S-2°N) in individual models with ORAS5. Models such as NorESM2-MM, MIROC6, INM-CM5, and E3SM1-1 are most skilful in representing the vertical structure of equatorial zonal currents (Figure 9c3). The CMIP6 models generally well simulate the subsurface zonal velocity maximum of equatorial currents accurately; however, their vertical extension is noted to be unrealistic compared to ORAS5.

3.3 Intercomparison of equatorial currents in reanalysis and CMIP6 models

In this section, we explore the vertical structure of the equatorial current systems such as Equatorial undercurrent (EUC), North Equatorial Current (NEC) and South Equatorial Current (SEC) in the Ocean reanalysis and as well as CMIP6 MMM. Unlike the other ocean basins, the EUC of the Indian Ocean is transient due to the lack of sustained easterlies (Reppin et al. 1999, Schott et al. 2009). The EUCs are generally eastward currents in the subsurface equatorial Indian Ocean found during boreal winter-spring (February-April) and summer-fall (August - October) months (Schott and McCreary 2001, Gnanaseelan and Deshpande, 2018). The former is associated with the upwelling Kelvin waves along the equator driven by the easterly winds and the latter is attributed to both the equatorial Kelvin waves and Rossby waves radiated from the eastern boundary (Iskandar et al. 2009, Chen et al., 2015). The westwards EUCs are less dominant and Huang et al. (2022) illustrated the existence of westward EUC during concurrent events of negative IOD and La Nina. Figure 10 shows the vertical distribution of zonal currents averaged over 2°S – 2°N in the upper 500m. It is worth noting that the core location of EUC is not consistent in reanalysis products. Previous studies based on ADCP observations of the equatorial Indian Ocean have documented the presence and variability of EUCs at depths of 50 – 200m (e.g., Reppin et al. 1999, Neiman et al. 2018, Schott et al. 1997). Based on RAMA observations, Chen et al. (2015) showed that the maximum velocity of the EUC in the western IO can reach up to 0.75 m/s during February to April. A well-defined core of EUC can be seen between 50-150m depth range in 50° – 70°E in ORAS5, SODA, and BRAN products (Figure 10b, f). Whereas, the core depth of EUC is not well distinguishable in other reanalysis datasets. In ECCO, the depth of the strong velocity core is shallower eastward, while the vertical extension of core velocity of EUC is much deeper in the central equatorial Indian Ocean in GODAS and ECDA products.

Figure 11 shows the diversity of reanalysis products in representing the climatological mean state of zonal currents averaged between 2°-5°N. Very recently, Sharma et al. (2023) considered the currents averaged over this location to examine the variability of NEC. The westward NEC from surface to a depth of 150m along the longitude stretch of 50°-90°E can be seen in GODAS (Figure 11a). Whereas, its location is confined to subsurface depth range of 50-150m in ECDA (Figure 11d). More or less similar representation of NEC system can be seen in other reanalysis products. It is to be noted that the subsurface currents in the ECDA product is limited to 200m depth. The subsurface strong velocity cores in them are located between 100-150m depth at 50° – 55°E and 80° – 85°E longitude bands (Figure 11b, c, e, f). We consider the climatology of zonal currents averaged between 7°-15°S to show the distribution of SEC system and it has similar representation in all the reanalysis products considered in the study (Figure 12). Previous studies have shown that the velocity of horizontally

flowing SEC increases gradually from east to west and stronger currents are observed at western boundary, near the east of Madagascar (e.g., Schott et al. 2001). All the reanalysis products show westward intensification of SEC between 45° -50°E, and the vertical extension of strong velocity core has marginal variation in them. The south equatorial undercurrent is distinguishable only in ORAS5, BRAN, and SODA. This transient current system mainly occurs from January to June, and gradually weakens in July and August (Chen et al. 2022).

Figure 13a shows the vertical structure of EUC in CMIP6 MMM and well-defined core velocity centred around 100°E as in ORAS5, GODAS, and BRAN. Models including INM-CM4-8, E3SM-1-1-ECA, MPI-ESM-1-2-HR, and ACCESS-CM2 were shown to have higher skill in representing the vertical structure of EUC (Figure. 13a2). Li et al. 2023 attributed Indian Ocean EUC biases to errors associated with the westward extension of the equatorial Pacific cold tongue and associated walker circulation changes. The enhanced Walker circulation over the Indo-Pacific Ocean directly causes a low-level westerly wind bias over the equatorial Indian Ocean and drives a shallow west–deep east thermocline tilt bias, leading to weak EUC in the Indian Ocean through wind-induced thermocline processes. The NEC system shows a large spread in CMIP6 models as 35% of models show negative PCC values (Figure. 13b2). This may be partially due to the uncertainties in ORAS5 in representing the vertical structure of NEC. It is to be noted that NEC simulated by NorESM2-MM, NorESM2-LM, and GISS-E2-1-G-CC are consistent with ORAS5 as indicated by the highest PCC and lowest RMSE values. The simulation of SEC is fairly consistent in MMM and individual models (Figure. 13c1 & c2). 39 models are skilful in representing the vertical structure of SEC as they characterise PCC values ranging between 0.68-0.98 and the RMSE values below 0.04. All the FGOALS and CESM2 models exhibit a large spread in simulating the SEC system.

3.4 Volume Transport variability

The distribution of heat and salt in the Tropical Indian Ocean is mainly driven by the interbasin exchange of waters in the eastern and western boundaries of the basin. In the eastern side of the basin, the ITF is a major passage to exchange the waters from Pacific to Indian Ocean. Similarly, in the western side, The AL is a major contributor to discharge the warm waters to the Atlantic and the Southern Latitudes of the Indian Ocean. Therefore, we explore the interbasin transport of waters in reanalysis datasets and CMIP6 models. Following Makarim et al. (2019), we consider a meridional section at 115°E and along 10.5°S – 15.5°S to compute the ITF volume transport from surface to 700m depth (Figure. S1). Annual mean transport estimated along this section is found to be $17 \pm 6 \text{ Sv}$ ($1\text{Sv} = 10^6 \text{ m}^3\text{s}^{-1}$) in ORAS5 and is consistent with previous direct estimates (Gordon et al. 2010, Sprintall

et al. 2009). Earlier estimates of ITF volume transport based on observations, reanalysis, and models range from 8Sv to 15Sv (e.g., Godfrey, 1996, Sprintall et al. 2005). The El Niño and positive Indian Ocean Dipole (IOD) mode events were found to have a strong influence on ITF with enhanced inflow to the Indian Ocean which led to a strengthened SEC system (Meyers, 1996; Liu et al. 2015; van Sebille et al. 2014). The International Nusantara Stratification and Transport (INSTANT) measurements estimate an approximate volume transport of 15 ± 6 Sv from the western Pacific to the southeast Indian Ocean (Gordon et al. 2010). Dong and McPhaden (2016) estimated ITF along the XBT line in the southeastern Indian Ocean at 113°E and along $8^\circ - 25^\circ\text{S}$ and they also found a similar estimate of volume transport. ITF estimated from BRAN shows lowest volume transport and highest variability among the reanalysis products (Figure. 14). The seasonal distribution has similar pattern in all the datasets and they characterise strongest westward volume transport during May-September.

The seasonal climatology of AL transport in various reanalysis products are shown in Figure 15. The strength of the transport and the shape of the seasonal cycle are highly inconsistent in them. Based on in situ Lagrangian subsurface floats and surface drifter measurements, Richardson (2007) found an AL transport of 14 - 16.6Sv between the surface and 1000m and has been considered as the best estimate of AL transport. The Agulhas transport estimated for the period 1958 -2009 shown to have distribution between 34-47Sv in ORAS4 dataset (Makarim et al. 2019). The southward volume transport by warm and salty surface and intermediate water by the Agulhas Current is estimated to be 84 ± 24 Sv based on observations (Lutjeharms et al. 2006, Beal and Elipot et al. 2016). The volume transport through the Mozambique Channel (16.7 ± 15.8 Sv; Ullgren et al. 2012) and by the southeast Madagascar Current (37 ± 10 Sv; Nauw et al. 2008) are the main sources of Agulhas transport. We show large values of volume transport in BRAN, ORAS5, and SODA and they also characterize large variability in seasonal cycle (Figure. 12a, b, e). Recently, Russo et al. (2022) showed that misinterpretation of vertical structure of currents in BRAN leads to large overestimation of magnitude of southwestward Agulhas leakage transport in BRAN although it is skillful in resolving the variability of Agulhas meanders. Reanalysis products show large uncertainty in representing ITF and AL transport. When compared to the magnitude of annual mean transport, the variability of AL transports in reanalysis are less compared to ITF in them.

The seasonal cycle of the ITF is estimated from 45 CMIP6 models are shown in Figure 16a. While the majority of CMIP6 models capture the shape of the seasonal cycle, there is significant variation in magnitude, particularly during the boreal winter months. The substantial inter-model

spread in simulating ITF transport in individual CMIP6 models results in a large underestimation of the volume transport in the multi-model mean (MMM) compared to ORAS5. The spread among the models in simulating the AL is found to be 11 Sv, and the majority of the models fail to represent the observed seasonal cycle. The skill of models in simulating the AL depends on their eddy-resolving characteristics (Marsh et al. 2000). Satellite observations provide strong evidence of increasing global surface eddy kinetic energy (Martínez-Moreno et al., 2021; Beech et al., 2022) and surface eddy heat flux (Guo et al., 2022). The changes in eddy kinetic energy in the Agulhas region can offer insights into local ocean circulation and Agulhas retroflection and Agulhas leakage transport variability. The significant projected intensification of eddy activity from the southern coast of Africa into the South Atlantic in the warming climate lead to intensified Agulhas leakage (Beech et al., 2022). Using satellite observations, Guo et al. (2022) showed a 17% increase in surface meridional eddy heat flux in the Agulhas return current. The magnitude of eddy kinetic energy variability is accurately resolved in a few CMIP6 models but is underrepresented when compared to observations (Beech et al., 2022). CMIP6 models majorly underestimate and show large uncertainty in representing AL strength (Figure 16b) Consequently, the amplitude of the AT seasonal cycle is systematically much smaller in MMM compared to reanalysis.

The understanding of the circulation bias and its rectification is a multifaceted challenge due to its dependence on coupled processes within both the ocean and atmosphere. The interactions between these components are complex, and biases in one component can propagate to others, leading to systematic bias in a climate model making it less confident for making future projections. For example, biases in ocean circulation can influence atmospheric circulation patterns, which in turn affect SSTs, leading to a feedback loop that potentially exacerbates biases in the ocean-atmosphere system. Furthermore, disentangling whether biases arise from inaccuracies in model representations of physical processes or from a lack of model resolution involves extensive efforts towards model-by-model evaluation. Addressing these challenges requires a comprehensive approach that involves improving both observational datasets and assessment of model representations of relevant processes. Enhanced observational networks, including satellite observations and in situ measurements, can provide valuable data for model evaluation.

4. Summary and Conclusions

The present study evaluates and intercompares the ocean currents in various reanalysis products such as ORAS5, ECCO, GODAS, ECDA, BRAN and SODA with reference to OSCAR and the equatorial RAMA moorings. It is to be noted that the reanalysis products are constructed using different ocean general circulation models constrained by various data assimilation techniques incorporating satellite

observations and in situ data from multiple sources. These global reanalysis products serve as boundary conditions for a range of regional ocean models, facilitating the study of specific oceanic processes and enabling ocean state forecasts for various applications. Different reanalysis products exhibit biases and uncertainties in representing the circulation features of the tropical Indian Ocean. Evaluation and intercomparison of upper ocean circulation features across these products can offer valuable insights for ocean modelers focusing on the Indian Ocean region, aiding them in selecting the most suitable product for boundary forcing. Incorporating the skilful reanalysis products as boundary conditions lead to more realistic simulations, which are crucial for various applications such as weather forecasting, climate studies, and marine resource management. In this context, present study documents the differences that exist in various reanalysis products in representing major circulation features of the tropical Indian Ocean. Further, the historical simulations of surface circulation in 45 climate models are compared with OSCAR product. The study also assesses the upper ocean vertical profile of zonal currents in few selected locations in these climate models.

All the reanalysis products represent the mean state of surface circulation realistically, especially in BRAN, ORAS5 and ECCO. However, they are diverse in representing the equatorial current system as shown by the spatial distribution of bias in their climatological mean state. We show that BRAN is the most skilful in representing the surface circulation of TIO, followed by ORAS5 as they characterize high PCC and low RMSE values, and GODAS is found to be less skilful in representing the climatological mean state of zonal currents over the tropical Indian Ocean for the period 1993-2017. The mean seasonal cycle of the zonal velocity in RAMA observations and reanalysis are constructed based on the availability of measurements from the equatorial region and the south Indian Ocean. The two strong eastward WJs can be observed in the equatorial moorings and the spring jets are deeper than the fall jets although the latter is climatologically stronger than the former. The semiannual WJs are well captured in all the reanalysis products but their vertical extension during both spring and fall seasons are different in various products. The magnitude and vertical distribution of spring WJs in the three locations are well simulated in BRAN whereas, the fall jets are misrepresented in it compared to the in-situ observations. The fall jets in the three locations are better represented in ECCO and ORAS5, but the spring jets are not well captured in the former. We show that the equatorial subsurface currents are better represented in ORAS5 compared to other reanalysis products. Although BRAN is most skillful in representing the surface circulation of TIO, the vertical distribution of subsurface currents in the upper layers are not well simulated in it. The higher skill of BRAN in representing surface zonal currents is attributed to a multi-scale data assimilation approach and an increased number of observations, including along-track altimeter sea level anomalies, as well

as the finest horizontal resolution. ORAS5 and ECCO also assimilate altimeter SLAs and characterize higher horizontal resolution.

Karmakar et al. (2018) assessed four reanalysis products, namely GODAS, ECDA, ORAS4, and SODA, revealing that ORAS4 exhibits realistic representation of surface circulation compared to the other reanalyses. However, it's worth noting that its upgraded version ORAS5 comprises enhanced horizontal and vertical resolution, improved parameterizations, additional perturbations in forcing, an ensemble approach bias correction technique, and assimilation of a greater number of observations when compared to its predecessor, ORAS4. The present study highlights the superior skill of the BRAN reanalysis product in representing the mean state of surface circulation, demonstrating its superiority over ORAS5. Among all the reanalysis products considered, ORAS5 has the highest vertical resolution and is found to be skillful in representing subsurface zonal currents at the equator. We also evaluate ECCO, which is another notable missing product in their study and we show that ECCO is skillful for TIO surface circulation followed by BRAN, and ORAS5.

We also evaluate climatological distribution NEC, EUC, and SEC systems in reanalysis products. The zonal currents averaged over 2° - 5° N and their vertical distribution in the subsurface layers are constructed to intercompare the NEC system in reanalysis products. The westward NEC from the surface to a depth of 150m along the longitude stretch of 50° - 90° E is observed in various reanalysis products. A more or less similar distribution of NEC with subsurface cores centred at 100m depth is observed in ORAS5, BRAN, and SODA datasets. The zonal currents averaged over 2° S – 2° N are considered to intercompare the EUC system in reanalysis. A well-defined core of EUC can be seen between 50-150m depth range in 50° – 70° E in ORAS5, SODA, and BRAN products. Whereas, the core depth of EUC is not well distinguishable in other reanalysis datasets. We consider the climatology of zonal currents averaged between 7° - 15° S to show the distribution of the SEC system and it has similar representation in all the reanalysis products considered in the study. All the reanalysis products show westward intensification of SEC between 45° - 50° E, and the vertical extension of strong velocity core has marginal variation in them. Reanalysis products show large uncertainty in inter-model volume transport of the Indian Ocean with Pacific through ITF and Atlantic through AL transport. The volume transport of ITF estimated from ORAS5 is found to be consistent with previous direct estimates whereas AL transport is highly inconsistent in reanalysis products.

While previous studies have investigated various physical processes of the Indian Ocean in past and latest generations of climate models, assessment of mean state and variability of currents have been overlooked in recent years. In this paper, we also evaluate surface circulation in historical simulations of 45 climate models relative to the OSCAR product. For most of the CMIP6 models considered in the

present study, the inter-model consistency of climatological mean state can be found. However, large deviations have been seen in models, including FGOALS-f3-L, FGOALS-g3-L, MIROC6, etc. We find that the NorESM2-MM model is the best in representing mean state of circulation over TIO, while the FGOALS-g3 turns out to be the least skillful. Multi model mean of the 45 CMIP6 models largely underestimate the volume transport of ITF with reference to ORAS5. The CMIP6 models are found to be problematic in simulating the equatorial currents and the strength of the south equatorial currents.

The quantification of errors in vertical current structure compared with in situ products are still lacking due to limitations in their availability and durations of measurements in them. This study recommends the importance of assessing specific current systems in various reanalysis products against observations. The biases discussed in surface currents in climate models may be indicative of their deficiency in simulating subsurface circulation features. Recently, Li et al. (2023) documented errors in both CMIP5 and CMIP6 models in representing the EUC system of the Indian Ocean and their link to the westward extended strong cold tongue bias of the equatorial Pacific. Quantification of errors in subsurface circulation of TIO and interoceanic transport requires further systematic assessment. The relative contribution of mean state biases of air-sea parameters and errors in physical processes in driving circulation biases in climate models will be addressed in future research. The results of the evaluation presented in this study would complement the existing understanding on the CMIP6 model's performance skill in representing the mean state of TIO. However, the present study focused on the climatological features of surface currents and vertical structure in the equatorial region from reanalysis and CMIP6 models. Many previous studies have focused on the interannual variability of zonal currents in the Indian Ocean (Gnanaseelan et al., 2012; Zhang et al., 2014; Deshpande et al., 2017). However, there is no consensus study on the performance of CMIP6 models in representing the Indian Ocean circulation variability, especially their mean-state bias impact on interannual variability. The present analysis is limited to focusing on the climatological mean features, and the interannual variability of surface and vertical sections of currents in the Indian Ocean in CMIP6 models will be explored in a detailed follow-up study. This paper will provide an important reference for further research on Indian Ocean circulation and also will serve as one of the baseline studies for evaluating future generations of CMIP models.

Author Contributions

Bhanu Deepika P: data curation; formal analysis; visualization; investigation; writing – original draft. **Soumya Mohan:** Conceptualization; methodology; investigation; writing – original draft. **Srinivas G:** Conceptualization; methodology; writing – review and editing.

Funding Information

The research is supported by funding from SERB-SRG grant (SRG/2021/000870).

Data Availability Statement

OSCAR and reanalysis products are downloaded from <http://apdrc.soest.hawaii.edu/>, <https://cds.climate.copernicus.eu/>, <ftp://ecco.jpl.nasa.gov/Version4/> Release3, <https://dapds00.nci.org.au/thredds/catalog/gb6/BRAN/BRAN2020/month/catalog.html?dataset=gb6/BRAN/BRAN2020/month>, <https://www.psl.noaa.gov/data/gridded/data.godas.html>. CMIP6 historical simulations of surface currents are downloaded from <https://data.ceda.ac.uk/badc/cmip6> & <https://esgf-node.llnl.gov/projects/cmip6>.

Conflict Of Interest Statement

The authors declare that they have no known conflicts of interest/competing interests.

Acknowledgements

The authors thank the Director CSIR-National Institute of Oceanography (NIO) for providing necessary computational facilities. Authors acknowledge funding from SERB-SRG grant (SRG/2021/000870). The authors are grateful to various reanalysis and CMIP6 repositories (<https://data.ceda.ac.uk/badc/cmip6> & <https://esgf-node.llnl.gov/projects/cmip6/>) This is NIO contribution number xxxx.

References

- Bao, Y., Song, Z., & Qiao, F. (2020). FIO-ESM version 2.0: Model description and evaluation. *Journal of Geophysical Research: Oceans*, 125(6), e2019JC016036.
- Beal, L. M., & Elipot, S. (2016). Broadening not strengthening of the Agulhas Current since the early 1990s. *Nature*, 540(7634), 570-573.
- Beal, L. M., De Ruijter, W. P., Biastoch, A., & Zahn, R. (2011). On the role of the Agulhas system in ocean circulation and climate. *Nature*, 472(7344), 429-436.
- Beech, N., Rackow, T., Semmler, T., Danilov, S., Wang, Q., & Jung, T. (2022). Long-term evolution of ocean eddy activity in a warming world. *Nature climate change*, 12(10), 910-917.
- Behringer, D. W., Ji, M., & Leetmaa, A. (1998). An improved coupled model for ENSO prediction and implications for ocean initialization. Part I: The ocean data assimilation system. *Monthly Weather Review*, 126(4), 1013-1021.
- Behringer, D., & Xue, Y. (2004, January). Evaluation of the global ocean data assimilation system at NCEP: The Pacific Ocean. In Proc. eighth symp. on integrated observing and assimilation systems for atmosphere, oceans, and land surface.

- Bhattacharya, B., Mohanty, S., & Singh, C. (2022). Assessment of the potential of CMIP6 models in simulating the sea surface temperature variability over the tropical Indian Ocean. *Theoretical and Applied Climatology*, 148(1-2), 585-602.
- Bi, D., Dix, M., Marsland, S., O'farrell, S., Sullivan, A., Bodman, R., ... & Heerdegen, A. (2020). Configuration and spin-up of ACCESS-CM2, the new generation Australian community climate and earth system simulator coupled model. *Journal of Southern Hemisphere Earth Systems Science*, 70(1), 225-251.
- Bonjean, F., & Lagerloef, G. S. (2002). Diagnostic model and analysis of the surface currents in the tropical Pacific Ocean. *Journal of Physical Oceanography*, 32(10), 2938-2954.
- Boucher, O., Servonnat, J., Albright, A. L., Aumont, O., Balkanski, Y., Bastrikov, V., ... & Vuichard, N. (2020). Presentation and evaluation of the IPSL-CM6A-LR climate model. *Journal of Advances in Modeling Earth Systems*, 12(7), e2019MS002010.
- Boyer, T. P., Antonov, J. I., Baranova, O. K., Garcia, H. E., Johnson, D. R., Mishonov, A. V., ... & Levitus, S. (2013). *World ocean database 2013*.
- Burrows, S. M., Maltrud, M. E., Yang, X., Zhu, Q., Jeffery, N., Shi, X., ... & Leung, L. R. (2019, December). The DOE E3SM Coupled Model v1. 1 Biogeochemistry Configuration and Coupled Carbon-Climate Experiments. In *AGU Fall Meeting Abstracts (Vol. 2019, pp. B53K-2537)*.
- Cabanes, C., Grouazel, A., von Schuckmann, K., Hamon, M., Turpin, V., Coatanoan, C., ... & Le Traon, P. Y. (2012). The CORA dataset: validation and diagnostics of ocean temperature and salinity in situ measurements. *Ocean Science Discussions*, 9(2), 1273-1312.
- Carton, J. A., Chepurin, G. A., & Chen, L. (2018). SODA3: A new ocean climate reanalysis. *Journal of Climate*, 31(17), 6967-6983.
- Casey, K.S., Brandon, T.B., Cornillon, P., Evans, R., 2010. The past, present, and future of the AVHRR Pathfinder SST Program, in: Barale, V., Gower, J., Alberotanza, L. (Eds.), *Oceanography from Space: Revisited*, pp. 273– 287.
- Chai, T., & Draxler, R. R. (2014). Root mean square error (RMSE) or mean absolute error (MAE)?—Arguments against avoiding RMSE in the literature. *Geoscientific model development*, 7(3), 1247-1250.
- Chamberlain, M. A., Oke, P. R., Fiedler, R. A., Beggs, H. M., Brassington, G. B., & Divakaran, P. (2021a). Next generation of Bluelink ocean reanalysis with multiscale data assimilation: BRAN2020. *Earth System Science Data*, 13(12), 5663-5688.
- Chamberlain, M. A., Oke, P. R., Brassington, G. B., Sandery, P., Divakaran, P., & Fiedler, R. A. S. (2021b). Multiscale data assimilation in the Bluelink ocean reanalysis (BRAN). *Ocean Modelling*, 166, 101849.
- Chen, C. A., Hsu, H. H., & Liang, H. C. (2021). Evaluation and comparison of CMIP6 and CMIP5 model performance in simulating the seasonal extreme precipitation in the Western North Pacific and East Asia. *Weather and Climate Extremes*, 31, 100303.

- Chen, G., Han, W., Zu, T., Chu, X., & Chen, J. (2022). The deep-penetrating south equatorial undercurrent in the tropical South Indian Ocean. *Geophysical Research Letters*, 49(6), e2022GL098163.
- Chen, G., Wang, D., Han, W., Feng, M., Wang, F., Li, Y., ... & Gordon, A. L. (2020). The extreme El Niño events suppressing the intraseasonal variability in the eastern tropical Indian Ocean. *Journal of Physical Oceanography*, 50(8), 2359-2372.
- Chu, X., Han, W., Zhang, L., & Chen, G. (2022). Effects of climate modes on interannual variability of the equatorial currents in the Indian ocean. *Climate Dynamics*, 1-14.
- Danabasoglu, G. (2019). IPCC DDC: NCAR CESM2-WACCM model output prepared for CMIP6 CMIP amip.
- Danabasoglu, G., Lamarque, J. F., Bacmeister, J., Bailey, D. A., DuVivier, A. K., Edwards, J., ... & Strand, W. G. (2020). The community earth system model version 2 (CESM2). *Journal of Advances in Modeling Earth Systems*, 12(2), e2019MS001916.
- de Ruijter, W. D., Biastoch, A., Drijfhout, S. S., Lutjeharms, J. R. E., Matano, R. P., Pichevin, T., ... & Weijer, W. (1999). Indian-Atlantic interocean exchange: Dynamics, estimation and impact. *Journal of Geophysical Research: Oceans*, 104(C9), 20885-20910.
- Delworth, T. L., & Dixon, K. W. (2006). Have anthropogenic aerosols delayed a greenhouse gas-induced weakening of the North Atlantic thermohaline circulation?. *Geophysical Research Letters*, 33(2).
- Derber, J., & Rosati, A. (1989). A global oceanic data assimilation system. *Journal of physical oceanography*, 19(9), 1333-1347.
- Deshpande, A., Gnanaseelan, C., Chowdary, J. S., & Rahul, S. (2017). Interannual spring Wyrтки jet variability and its regional impacts. *Dynamics of Atmospheres and Oceans*, 78, 26-37.
- Dong, L., & McPhaden, M. J. (2016). Interhemispheric SST gradient trends in the Indian Ocean prior to and during the recent global warming hiatus. *Journal of Climate*, 29(24), 9077-9095.
- Döscher, R., Acosta, M., Alessandri, A., Anthoni, P., Arneth, A., Arsouze, T., ... & Zhang, Q. (2021). The EC-earth3 Earth system model for the climate model intercomparison project 6. *Geoscientific Model Development Discussions*, 2021, 1-90.
- Duan, Y., Liu, L., Han, G., Liu, H., Yu, W., Yang, G., ... & Waheed, H. (2016). Anomalous behaviors of Wyrтки Jets in the equatorial Indian Ocean during 2013. *Scientific Reports*, 6(1), 29688.
- ESR (2022) Ocean surface current analyses real-time (OSCAR) surface currents – final 0.25 degree (Version 2.0). Ver. 2.0 (CA, USA: PO.DAAC). Available at: <https://Doi.Org/10.5067/OSCAR-25F20> (Accessed 2023-01-12).
- Eyring, V., Bony, S., Meehl, G. A., Senior, C. A., Stevens, B., Stouffer, R. J., & Taylor, K. E. (2016). Overview of the Coupled Model Intercomparison Project Phase 6 (CMIP6) experimental design and organization. *Geoscientific Model Development*, 9(5), 1937-1958.

- Fairall, C. W., Bradley, E. F., Hare, J. E., Grachev, A. A., & Edson, J. B. (2003). Bulk parameterization of air–sea fluxes: Updates and verification for the COARE algorithm. *Journal of climate*, 16(4), 571-591.
- Feng, X., Wu, L., & Wang, C. (2023). Intermodel Biases of the Western North Pacific Monsoon Trough in CMIP6 Models. *Journal of Climate*, 36(15), 5281-5292.
- Forget, G. A. E. L., Campin, J. M., Heimbach, P., Hill, C. N., Ponte, R. M., & Wunsch, C. (2015). ECCO version 4: An integrated framework for non-linear inverse modeling and global ocean state estimation. *Geoscientific Model Development*, 8(10), 3071-3104.
- Fukumori, I., Wang, O., Fenty, I., Forget, G., Heimbach, P., & Ponte, R. M. (2017). ECCO version 4 release 3.
- Gnanaseelan, C., & Deshpande, A. (2018). Equatorial Indian Ocean subsurface current variability in an Ocean general circulation model. *Climate dynamics*, 50, 1705-1717.
- Godfrey, J. S. (1996). The effect of the Indonesian throughflow on ocean circulation and heat exchange with the atmosphere: A review. *Journal of Geophysical Research: Oceans*, 101(C5), 12217-12237.
- Gordon, A. L. (2001). Interocean exchange. In *International Geophysics* (Vol. 77, pp. 303-314). Academic Press.
- Gordon, A. L. (2005). The Indonesian seas. *Oceanography*, 18(4), 14.
- Gordon, A. L., Sprintall, J., Van Aken, H. M., Susanto, D., Wijffels, S., Molcard, R., ... & Wirasantosa, S. (2010). The Indonesian throughflow during 2004–2006 as observed by the INSTANT program. *Dynamics of Atmospheres and Oceans*, 50(2), 115-128.
- Gordon, A. L., Susanto, R. D., Field, A., Huber, B. A., Pranowo, W., & Wirasantosa, S. (2008). Makassar Strait throughflow, 2004 to 2006. *Geophysical Research Letters*, 35(24).
- Guangqing, Z., Yunquan, Z., Jinrong, J., He, Z., Baodong, W., Hang, C., ... & Minghua, Z. (2020). Earth system model: CAS-ESM. *Frontiers of Data and Computing*, 2(1), 38-54.
- Guo, H., John, J. G., Blanton, C., McHugh, C., Nikonov, S., Radhakrishnan, A., ... & Zhang, R. (2018). NOAA-GFDL GFDL-CM4 model output historical. *Earth System Grid Federation*, 10.
- Guo, Y., Bachman, S., Bryan, F., & Bishop, S. (2022). Increasing trends in oceanic surface poleward eddy heat flux observed over the past three decades. *Geophysical Research Letters*, 49(16), e2022GL099362.
- Gutjahr, O., Putrasahan, D., Lohmann, K., Jungclaus, J. H., von Storch, J. S., Brüggemann, N., ... & Stössel, A. (2019). Max planck institute earth system model (MPI-ESM1. 2) for the high-resolution model intercomparison project (HighResMIP). *Geoscientific Model Development*, 12(7), 3241-3281.
- Halder, S., Parekh, A., Chowdary, J. S., Gnanaseelan, C., & Kulkarni, A. (2021). Assessment of CMIP6 models' skill for tropical Indian Ocean sea surface temperature variability. *International Journal of Climatology*, 41(4), 2568-2588.
- Han, W., Lawrence, D. M., & Webster, P. J. (2001). Dynamical response of equatorial Indian Ocean to intraseasonal winds: Zonal flow. *Geophysical Research Letters*, 28(22), 4215-4218.

- Han, W., McCreary, J. P., Anderson, D. L. T., & Mariano, A. J. (1999). Dynamics of the eastern surface jets in the equatorial Indian Ocean. *Journal of Physical Oceanography*, 29(9), 2191-2209.
- He, B., Bao, Q., Wang, X., Zhou, L., Wu, X., Liu, Y., ... & Zhang, X. (2019). CAS FGOALS-f3-L model datasets for CMIP6 historical atmospheric model intercomparison project simulation. *Advances in Atmospheric Sciences*, 36, 771-778.
- Hewitt, H. T., Roberts, M., Mathiot, P., Biastoch, A., Blockley, E., Chassignet, E. P., ... & Zhang, Q. (2020). Resolving and parameterising the ocean mesoscale in earth system models. *Current Climate Change Reports*, 6, 137-152.
- Horii, T., Ueki, I., Ando, K., & Mizuno, K. (2013). Eastern Indian Ocean warming associated with the negative Indian Ocean dipole: A case study of the 2010 event. *Journal of Geophysical Research: Oceans*, 118(1), 536-549
- Huang, Wenyu (2019). THU CIESM model output prepared for CMIP6 ScenarioMIP..Earth System Grid Federation. <https://doi.org/10.22033/ESGF/CMIP6.1357>
- Ji, M., Leetmaa, A., & Derber, J. (1995). An ocean analysis system for seasonal to interannual climate studies. *Monthly Weather Review*, 123(2), 460-481.
- Johnson, E. S., Bonjean, F., Lagerloef, G. S., Gunn, J. T., & Mitchum, G. T. (2007). Validation and error analysis of OSCAR sea surface currents. *Journal of Atmospheric and Oceanic Technology*, 24(4), 688-701.
- Joseph, S., Wallcraft, A. J., Jensen, T. G., Ravichandran, M., Shenoi, S. S. C., & Nayak, S. (2012). Weakening of spring Wyrтки jets in the Indian Ocean during 2006–2011. *Journal of Geophysical Research: Oceans*, 117(C4).
- Karmakar, A., Parekh, A., Chowdary, J. S., & Gnanaseelan, C. (2018). Inter comparison of Tropical Indian Ocean features in different ocean reanalysis products. *Climate Dynamics*, 51, 119-141.
- Kelley, M., Schmidt, G. A., Nazarenko, L. S., Bauer, S. E., Ruedy, R., Russell, G. L., ... & Yao, M. S. (2020). GISS-E2. 1: Configurations and climatology. *Journal of Advances in Modeling Earth Systems*, 12(8), e2019MS002025.
- Knutti, R., & Sedláček, J. (2013). Robustness and uncertainties in the new CMIP5 climate model projections. *Nature climate change*, 3(4), 369-373.
- Knutti, R., Furrer, R., Tebaldi, C., Cermak, J., & Meehl, G. A. (2010). Challenges in combining projections from multiple climate models. *Journal of Climate*, 23(10), 2739-2758.
- Krishnan, A., & Bhaskaran, P. K. (2020). Skill assessment of global climate model wind speed from CMIP5 and CMIP6 and evaluation of projections for the Bay of Bengal. *Climate Dynamics*, 55(9-10), 2667-2687.
- Kumar, D., & Ganguly, A. R. (2018). Intercomparison of model response and internal variability across climate model ensembles. *Climate dynamics*, 51(1-2), 207-219.
- Lagerloef, G. S., Mitchum, G. T., Lukas, R. B., & Niiler, P. P. (1999). Tropical Pacific near-surface currents estimated from altimeter, wind, and drifter data. *Journal of Geophysical Research: Oceans*, 104(C10), 23313-23326.

- Large, W., & Yeager, S. G. (2009). The global climatology of an interannually varying air–sea flux data set. *Climate dynamics*, 33, 341-364.
- Levitus, S., Burgett, R., & Boyer, T. P. (1994). *World Ocean Atlas 1994*. Vol. 3, Salinity.
- Li, J., Xu, K., Wang, W., He, Z., & Huang, K. (2023). Biases and improvements of the boreal winter–spring equatorial undercurrent in the Indian Ocean in the CMIP5 and CMIP6 models. *Frontiers in Marine Science*, 10, 1168385.
- Li, J., Xu, K., Wang, W., He, Z., & Huang, K. (2023). Biases and improvements of the boreal winter–spring equatorial undercurrent in the Indian Ocean in the CMIP5 and CMIP6 models. *Frontiers in Marine Science*, 10, 1168385.
- Li, L., Yu, Y., Tang, Y., Lin, P., Xie, J., Song, M., ... & Wei, J. (2020). The flexible global ocean–atmosphere–land system model grid-point version 3 (FGOALS-g3): description and evaluation. *Journal of Advances in Modeling Earth Systems*, 12(9), e2019MS002012.
- Lin, Y. S., Wang, L. C., & Li, J. L. F. (2023). Effects of equatorial ocean current bias on simulated El Niño pattern in CMIP6 models. *Geophysical Research Letters*, 50(8), e2023GL102890.
- Lin, Y., Huang, X., Liang, Y., Qin, Y., Xu, S., Huang, W., ... & Gong, P. (2020). Community integrated earth system model (CIesm): Description and evaluation. *Journal of Advances in Modeling Earth Systems*, 12(8), e2019MS002036.
- Liu, L., Liu, B., Han, G., Feng, L., Li, X., & Yu, W. (2016). Assessment of the seasonal variation of simulated Wyrki jet over the tropical Indian Ocean in CMIP5 models. *Arabian Journal of Geosciences*, 9, 1-9.
- Liu, Q. Y., Feng, M., Wang, D., & Wijffels, S. (2015). Interannual variability of the Indonesian Throughflow transport: A revisit based on 30 year expendable bathythermograph data. *Journal of Geophysical Research: Oceans*, 120(12), 8270-8282.
- Lutjeharms, J. R. (2006). *The Agulhas current retroflection* (pp. 151-207). Springer Berlin Heidelberg.
- Makarim, S., Sprintall, J., Liu, Z., Yu, W., Santoso, A., Yan, X. H., & Susanto, R. D. (2019). Previously unidentified Indonesian Throughflow pathways and freshening in the Indian Ocean during recent decades. *Scientific Reports*, 9(1), 7364.
- Marshall, J., Adcroft, A., Hill, C., Perelman, L., & Heisey, C. (1997). A finite-volume, incompressible Navier Stokes model for studies of the ocean on parallel computers. *Journal of Geophysical Research: Oceans*, 102(C3), 5753-5766.
- Martínez-Moreno, J., Hogg, A. M., England, M. H., Constantinou, N. C., Kiss, A. E., & Morrison, A. K. (2021). Global changes in oceanic mesoscale currents over the satellite altimetry record. *Nature Climate Change*, 11(5), 397-403.
- Mauritsen, T., Bader, J., Becker, T., Behrens, J., Bittner, M., Brokopf, R., ... & Roeckner, E. (2019). Developments in the MPI-M Earth System Model version 1.2 (MPI-ESM1. 2) and its response to increasing CO₂. *Journal of Advances in Modeling Earth Systems*, 11(4), 998-1038.

- McCarty, M.E., L.J. Mangum, and M.J. McPhaden, 1997: Temperature errors in TAO data induced by mooring motion. NOAA Tech. Memo. ERL PMEL-108, Pacific Marine Environmental Laboratory, Seattle, WA, 68 pp.
- McCreary, J. P., & Kundu, P. K. (1988). A numerical investigation of the Somali Current during the Southwest Monsoon. *Journal of marine research*, 46(1), 25-58.
- McGregor, S., Sen Gupta, A., Dommenget, D., Lee, T., McPhaden, M. J., & Kessler, W. S. (2017). Factors influencing the skill of synthesized satellite wind products in the tropical Pacific. *Journal of Geophysical Research: Oceans*, 122(2), 1072-1089.
- McKenna, S., Santoso, A., Sen Gupta, A., & Taschetto, A. S. (2024). Understanding biases in Indian Ocean seasonal SST in CMIP6 models. *Journal of Geophysical Research: Oceans*, 129(2), e2023JC020330.
- McKenna, S., Santoso, A., Gupta, A. S., Taschetto, A. S., & Cai, W. (2020). Indian Ocean Dipole in CMIP5 and CMIP6: characteristics, biases, and links to ENSO. *Scientific reports*, 10(1), 11500.
- McKenna, S., Santoso, A., Sen Gupta, A., & Taschetto, A. S. (2024). Understanding biases in Indian Ocean seasonal SST in CMIP6 models. *Journal of Geophysical Research: Oceans*, 129(2), e2023JC020330.
- McPhaden, M. J., Foltz, G. R., Lee, T., Murty, V. S. N., Ravichandran, M., Vecchi, G. A., ... & Yu, L. (2009). Ocean-atmosphere interactions during cyclone nargis. *EOS, Transactions American Geophysical Union*, 90(7), 53-54.
- McPhaden, M. J., Wang, Y., & Ravichandran, M. (2015). Volume transports of the W yrkti jets and their relationship to the I ndian O cean D ipole. *Journal of Geophysical Research: Oceans*, 120(8), 5302-5317.
- Menemenlis, D., Fukumori, I., & Lee, T. (2005). Using Green's functions to calibrate an ocean general circulation model. *Monthly weather review*, 133(5), 1224-1240.
- Meyers, G. (1996). Variation of Indonesian throughflow and the El Niño-southern oscillation. *Journal of Geophysical Research: Oceans*, 101(C5), 12255-12263.
- Miller, R. L., Schmidt, G. A., Nazarenko, L. S., Bauer, S. E., Kelley, M., Ruedy, R., ... & Yao, M. S. (2021). CMIP6 historical simulations (1850–2014) with GISS-E2. 1. *Journal of Advances in Modeling Earth Systems*, 13(1), e2019MS002034.
- Mishra, S. K., Sahany, S., Salunke, P., Kang, I. S., & Jain, S. (2018). Fidelity of CMIP5 multi-model mean in assessing Indian monsoon simulations. *npj Climate and Atmospheric Science*, 1(1), 39.
- Nauw, J. J., Van Aken, H. M., Webb, A., Lutjeharms, J. R. E., & De Ruijter, W. P. M. (2008). Observations of the southern East Madagascar Current and undercurrent and countercurrent system. *Journal of Geophysical Research: Oceans*, 113(C8).
- Neiman, V. G., Frey, D. I., Ambrosimov, A. K., Kaplunenko, D. D., Morozov, E. G., & Shapovalov, S. M. (2018, March). Equatorial Currents in the Indian Ocean Based on Measurements in February 2017. In *Doklady Earth Sciences* (Vol. 479, pp. 358-361). Pleiades Publishing.

- Oke, P. R., Griffin, D. A., Schiller, A., Matear, R. J., Fiedler, R., Mansbridge, J., ... & Ridgway, K. (2013). Evaluation of a near-global eddy-resolving ocean model. *Geoscientific model development*, 6(3), 591-615.
- Pak, G., Noh, Y., Lee, M. I., Yeh, S. W., Kim, D., Kim, S. Y., ... & Kim, Y. H. (2021). Korea institute of ocean science and technology earth system model and its simulation characteristics. *Ocean Science Journal*, 56(1), 18-45.
- Pearson, J., Resplandy, L., & Poupon, M. (2022). Coastlines At risk of hypoxia from natural variability in the northern Indian ocean. *Global Biogeochemical Cycles*, 36(6), e2021GB007192.
- Penduff, T., Juza, M., Brodeau, L., Smith, G. C., Barnier, B., Molines, J. M., ... & Madec, G. (2010). Impact of global ocean model resolution on sea-level variability with emphasis on interannual time scales. *Ocean Science*, 6(1), 269-284.
- Phillips, H. E., Tandon, A., Furue, R., Hood, R., Ummenhofer, C. C., Benthuyzen, J. A., ... & Wiggert, J. (2021). Progress in understanding of Indian Ocean circulation, variability, air–sea exchange, and impacts on biogeochemistry. *Ocean Science*, 17(6), 1677-1751.
- Quartly, G. D., Buck, J. J., Srokosz, M. A., & Coward, A. C. (2006). Eddies around Madagascar—The retroreflection re-considered. *Journal of Marine Systems*, 63(3-4), 115-129.
- Rahaman, H., Venugopal, T., Penny, S. G., Behringer, D. W., Ravichandran, M., Raju, J. V. S., ... & Sengupta, D. (2019). Improved ocean analysis for the Indian Ocean. *Journal of Operational Oceanography*, 12(1), 16-33.
- Reppin, J., Schott, F. A., Fischer, J., & Quadfasel, D. (1999). Equatorial currents and transports in the upper central Indian Ocean: Annual cycle and interannual variability. *Journal of Geophysical Research: Oceans*, 104(C7), 15495-15514.
- Reynolds, R. W., Rayner, N. A., Smith, T. M., Stokes, D. C., & Wang, W. (2002). An improved in situ and satellite SST analysis for climate. *Journal of climate*, 15(13), 1609-1625.
- Richardson, P. L. (2007). Agulhas leakage into the Atlantic estimated with subsurface floats and surface drifters. *Deep Sea Research Part I: Oceanographic Research Papers*, 54(8), 1361-1389.
- Rong, X. (2019). IPCC DDC: CAMS CAMS_CSM1.0 model output prepared for CMIP6 CMIP.
- Russo, C. S., Veitch, J., Carr, M., Fearon, G., & Whittle, C. (2022). An intercomparison of global reanalysis products for Southern Africa's major oceanographic features. *Frontiers in Marine Science*, 9, 837906.
- Saha, S., Nadiga, S., Thiaw, C., Wang, J., Wang, W., Zhang, Q., ... & Xie, P. (2006). The NCEP climate forecast system. *Journal of Climate*, 19(15), 3483-3517.
- Sajidh, C.K., Chatterjee, A. Indian Ocean dynamic sea level, its variability and projections in CMIP6 models. *Clim Dyn* (2023). <https://doi.org/10.1007/s00382-023-06676-z>
- Sakov, P. (2014). EnKF-C user guide. arXiv preprint arXiv:1410.1233.
- Schmitz Jr., W. J.: On the interbasin-scale thermohaline circulation, *Rev. Geophys.*, 33, 151–173, <https://doi.org/10.1029/95RG00879>, 1995.

- Schott, F. (1983). Monsoon response of the Somali Current and associated upwelling. *Progress in oceanography*, 12(3), 357-381.
- Schott, F. A., & McCreary Jr, J. P. (2001). The monsoon circulation of the Indian Ocean. *Progress in Oceanography*, 51(1), 1-123.
- Schott, F. A., Xie, S. P., & McCreary Jr, J. P. (2009). Indian Ocean circulation and climate variability. *Reviews of Geophysics*, 47(1).
- Schott, F., Fischer, J., Gartnericht, U., & Quadfasel, D. (1997). Summer monsoon response of the northern Somali Current, 1995. *Geophysical Research Letters*, 24(21), 2565-2568.
- Seland, Ø., Bentsen, M., Olivié, D., Toniazzo, T., Gjermundsen, A., Graff, L. S., ... & Schulz, M. (2020). Overview of the Norwegian Earth System Model (NorESM2) and key climate response of CMIP6 DECK, historical, and scenario simulations. *Geoscientific Model Development*, 13(12), 6165-6200.
- Seland, Ø., Bentsen, M., Olivié, D., Toniazzo, T., Gjermundsen, A., Graff, L. S., ... & Schulz, M. (2020). Overview of the Norwegian Earth System Model (NorESM2) and key climate response of CMIP6 DECK, historical, and scenario simulations. *Geoscientific Model Development*, 13(12), 6165-6200.
- Sepulchre, P., Caubel, A., Ladant, J. B., Bopp, L., Boucher, O., Braconnot, P., ... & Tardif, D. (2020). IPSL-CM5A2—an Earth system model designed for multi-millennial climate simulations. *Geoscientific Model Development*, 13(7), 3011-3053.
- Shankar, D., Vinayachandran, P. N., & Unnikrishnan, A. S. (2002). The monsoon currents in the north Indian Ocean. *Progress in oceanography*, 52(1), 63-120.
- Sharma, S., Ha, K. J., Yamaguchi, R., Rodgers, K. B., Timmermann, A., & Chung, E. S. (2023). Future Indian Ocean warming patterns. *Nature Communications*, 14(1), 1789.
- Shenoi, S. S. C., Saji, P. K., & Almeida, A. M. (1999). Near-surface circulation and kinetic energy in the tropical Indian Ocean derived from Lagrangian drifters. *Journal of Marine Research*, 57(6), 885-907.
- Sikhakolli, R., Sharma, R., Basu, S., Gohil, B. S., Sarkar, A., & Prasad, K. V. S. R. (2013). Evaluation of OSCAR ocean surface current product in the tropical Indian Ocean using in situ data. *Journal of earth system science*, 122, 187-199.
- Song, S., Zhang, X., & Yan, X. (2022). Evaluation of the Performance of CMIP6 Model Simulations for the Asian-Pacific Region: Perspectives from Multiple Dimensions.
- Sprintall, J., Gordon, A. L., Koch-Larrouy, A., Lee, T., Potemra, J. T., Pujiana, K., & Wijffels, S. E. (2014). The Indonesian seas and their role in the coupled ocean–climate system. *Nature Geoscience*, 7(7), 487-492.
- Sprintall, J., Wijffels, S. E., Molcard, R., & Jaya, I. (2009). Direct estimates of the Indonesian Throughflow entering the Indian Ocean: 2004–2006. *Journal of Geophysical Research: Oceans*, 114(C7).

- Swart, N. C., Cole, J. N., Kharin, V. V., Lazare, M., Scinocca, J. F., Gillett, N. P., ... & Winter, B. (2019). The Canadian earth system model version 5 (CanESM5. 0.3). *Geoscientific Model Development*, 12(11), 4823-4873.
- Taylor, R. (1990). Interpretation of the correlation coefficient: a basic review. *Journal of diagnostic medical sonography*, 6(1), 35-39.
- Tillinger, D., & Gordon, A. L. (2009). Fifty years of the Indonesian Throughflow. *Journal of Climate*, 22(23), 6342-6355.
- Tokarska, K. B., Stolpe, M. B., Sippel, S., Fischer, E. M., Smith, C. J., Lehner, F., & Knutti, R. (2020). Past warming trend constrains future warming in CMIP6 models. *Science advances*, 6(12), eaaz9549.
- Ullgren, J. E., van Aken, H. M., Ridderinkhof, H., & De Ruijter, W. P. M. (2012). The hydrography of the Mozambique Channel from six years of continuous temperature, salinity, and velocity observations. *Deep Sea Research Part I: Oceanographic Research Papers*, 69, 36-50.
- Utari, P. A. (2021, November). Observed of Equatorial Currents in the Indian Ocean during Two Contrasting IOD Events: 2006 and 2010. In *IOP Conference Series: Earth and Environmental Science* (Vol. 925, No. 1, p. 012007). IOP Publishing.
- Vaittinada Ayar, P., Battisti, D. S., Li, C., King, M., Vrac, M., & Tjiputra, J. (2023). A regime view of ENSO flavors through clustering in CMIP6 models. *Earth's Future*, 11(11), e2022EF003460.
- Valsala, V. K., & Ikeda, M. (2007). Pathways and effects of the Indonesian Throughflow water in the Indian Ocean using particle trajectory and tracers in an OGCM. *Journal of Climate*, 20(13), 2994-3017.
- Van Noije, T., Bergman, T., Le Sager, P., O'Donnell, D., Makkonen, R., Gonçalves-Ageitos, M., ... & Yang, S. (2021). EC-Earth3-AerChem: a global climate model with interactive aerosols and atmospheric chemistry participating in CMIP6. *Geoscientific Model Development*, 14(9), 5637-5668.
- van Sebille, E., Sprintall, J., Schwarzkopf, F. U., Sen Gupta, A., Santoso, A., England, M. H., ... & Böning, C. W. (2014). Pacific-to-Indian Ocean connectivity: Tasman leakage, Indonesian Throughflow, and the role of ENSO. *Journal of Geophysical Research: Oceans*, 119(2), 1365-1382.
- Volodin, E. M. (2013). The mechanism of multidecadal variability in the Arctic and North Atlantic in climate model INMCM4. *Environmental Research Letters*, 8(3), 035038.
- Volodin, E. M., Mortikov, E. V., Kostykin, S. V., Galin, V. Y., Lykosov, V. N., Gritsun, A. S., ... & Yakovlev, N. G. (2017). Simulation of modern climate with the new version of the INM RAS climate model. *Izvestiya, Atmospheric and Oceanic Physics*, 53, 142-155.
- Wang, Y. C., Hsu, H. H., Chen, C. A., Tseng, W. L., Hsu, P. C., Lin, C. W., ... & Shiu, C. J. (2021). Performance of the Taiwan earth system model in simulating climate variability compared with observations and CMIP6 model simulations. *Journal of Advances in Modeling Earth Systems*, 13(7), e2020MS002353.
- Wu, T., Lu, Y., Fang, Y., Xin, X., Li, L., Li, W., ... & Liu, X. (2019). The Beijing Climate Center Climate System Model (BCC-CSM): the main progress from CMIP5 to CMIP6. *Geoscientific Model Development*, 12(4), 1573-1600.

- Wyrtki, K. (1973). An equatorial jet in the Indian Ocean. *Science*, 181(4096), 262-264.
- Yang, M. A., Yang, C. U. I., Wen, Z. H. A. N. G., & Xin, L. I. (2023). Projection of the future temperature changes of Yellow River Basin Ningxia section based on CMIP6 models. *Journal of Arid Meteorology*, 41(1), 43.
- Yuhong, Z., Yan, D. U., & Haiming, X. U. (2012). Seasonal variability of the west-east water mass exchange on the section of central equatorial Indian Ocean and its regional difference, 34(2), 30-38.
- Yukimoto, S., Kawai, H., Koshiro, T., Oshima, N., Yoshida, K., Urakawa, S., ... & Ishii, M. (2019). The Meteorological Research Institute Earth System Model version 2.0, MRI-ESM2. 0: Description and basic evaluation of the physical component. *Journal of the Meteorological Society of Japan. Ser. II*, 97(5), 931-965.
- Zhang, J., & Wang, C. (2023). Zonal current structure of the Indian Ocean in CMIP6 models. *Deep Sea Research Part II: Topical Studies in Oceanography*, 208, 105260.
- Zhang, W., Jin, F. F., & Turner, A. (2014). Increasing autumn drought over southern China associated with ENSO regime shift. *Geophysical Research Letters*, 41(11), 4020-4026.
- Ziehn, T., Chamberlain, M. A., Law, R. M., Lenton, A., Bodman, R. W., Dix, M., ... & Srbinovsky, J. (2020). The Australian earth system model: ACCESS-ESM1. 5. *Journal of Southern Hemisphere Earth Systems Science*, 70(1), 193-214.
- Zuo, H., Balmaseda, M. A., & Mogensen, K. (2017). The new eddy-permitting ORAP5 ocean reanalysis: description, evaluation and uncertainties in climate signals. *Climate Dynamics*, 49, 791-811.
- Zuo, H., Balmaseda, M. A., Tietsche, S., Mogensen, K., & Mayer, M. (2019). The ECMWF operational ensemble reanalysis–analysis system for ocean and sea ice: a description of the system and assessment. *Ocean science*, 15(3), 779-808.

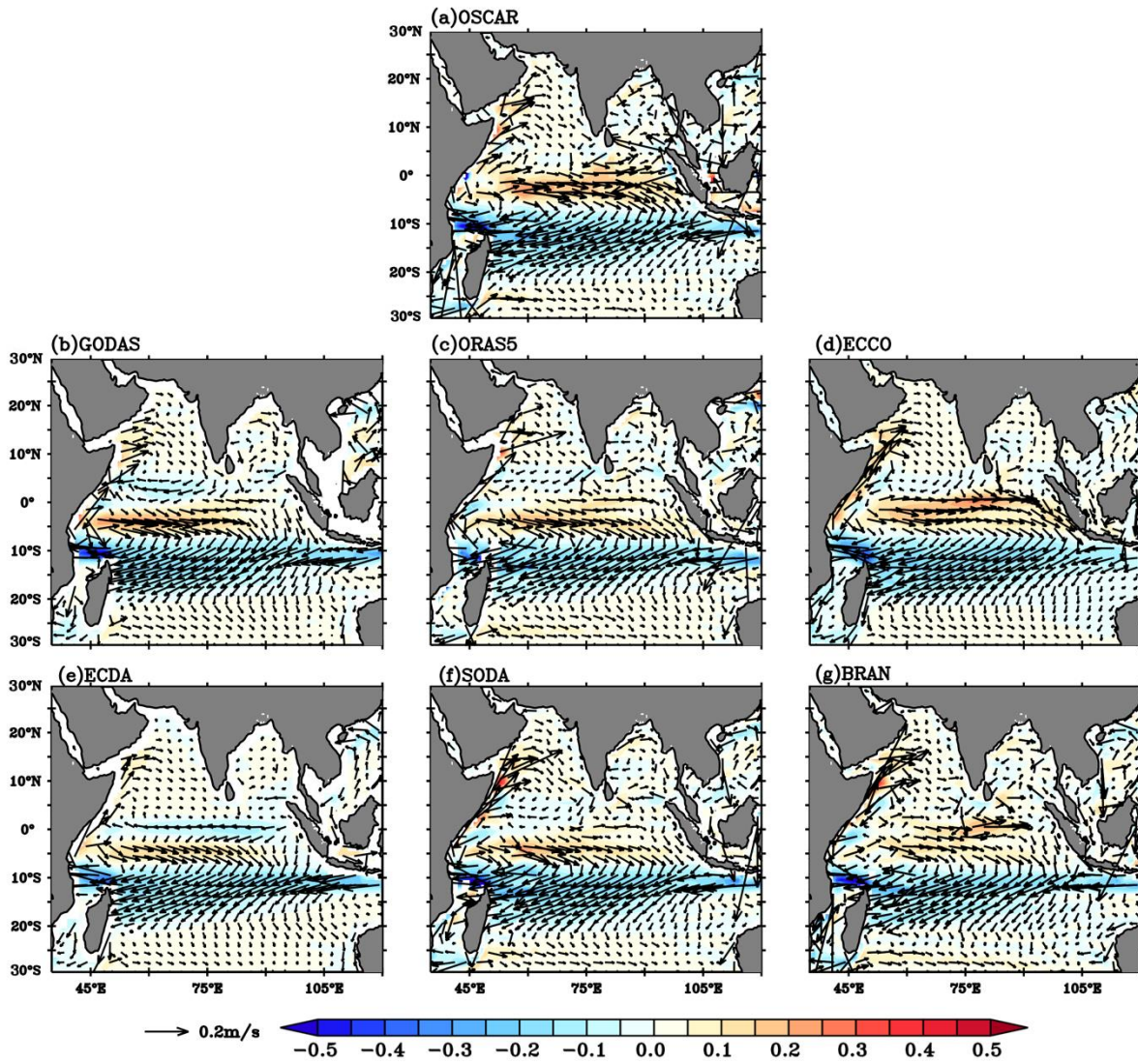


Fig. 1. The climatological mean of surface currents (m/s) averaged for upper 30m (u,v as vectors and shaded is u) from (a) OSCAR, (b) GODAS, (c) ORAs5, (d) ECCO, (e) ECDA, (f) SODA and (g) BRAN reanalysis products. The climatology is based on the period 1993 -2017 for all the products.

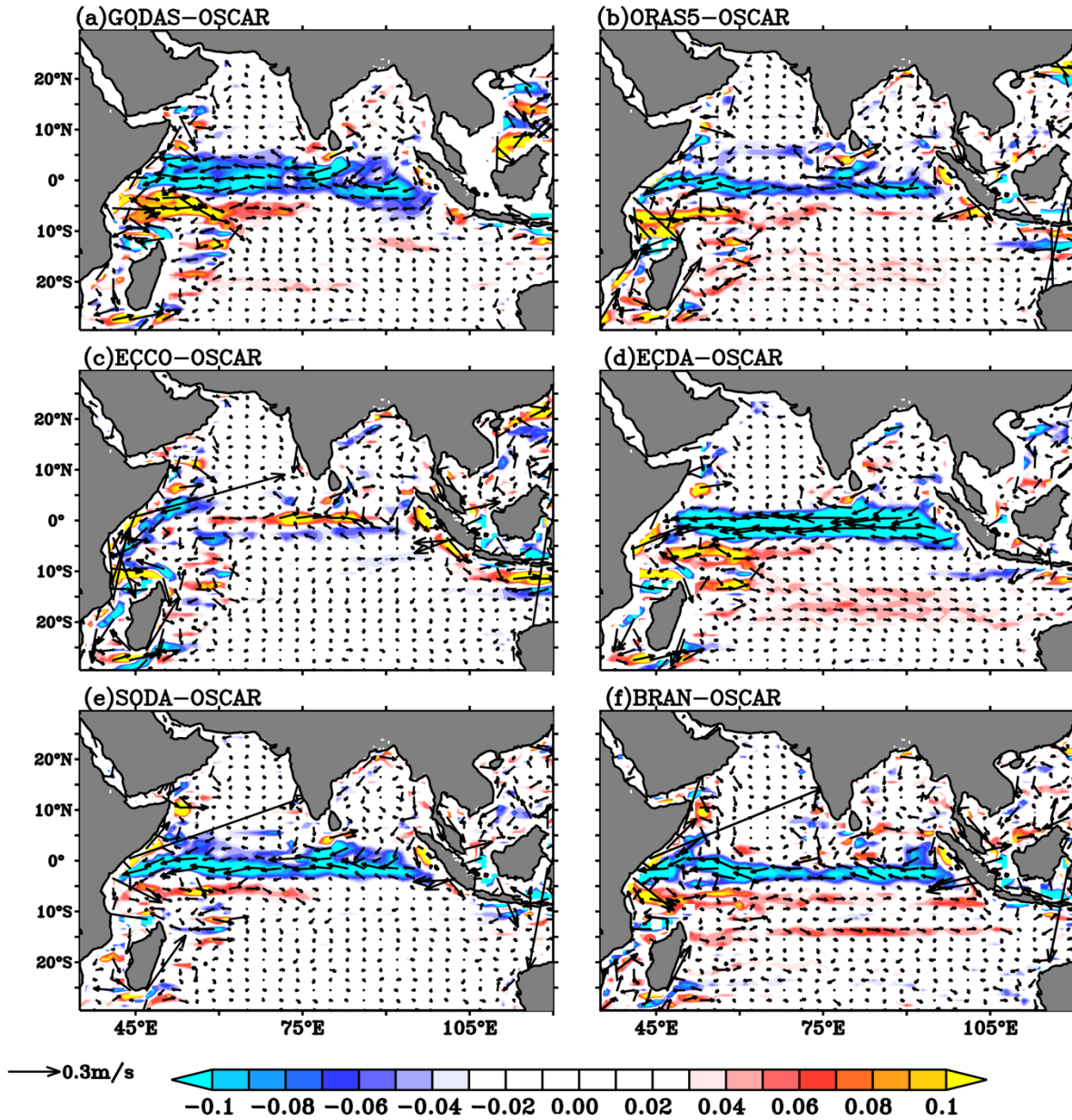


Fig. 2. The climatological mean biases (m/s) of surface currents (u,v as vectors and shaded is u) in (a) GODAS, (b) ORAS5, (c) ECCO, (d) ECDA, (e) SODA and (f) BRAN reanalysis with respect to OSCAR currents.

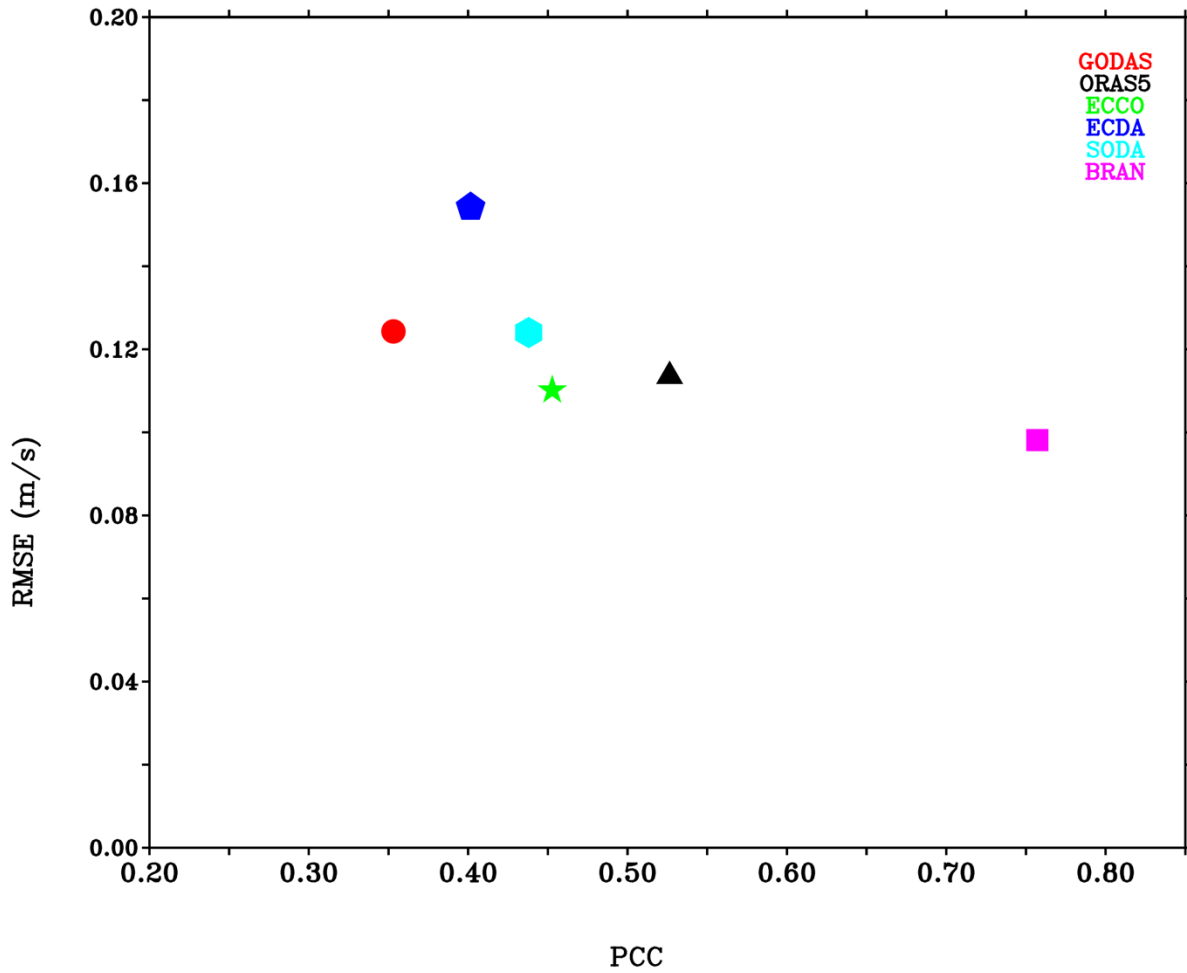


Fig. 3. The Scatterplot of PCC against RMSE (m/s) for annual climatology of Zonal Currents in all reanalysis Products with respect to OSCAR for the TIO region.

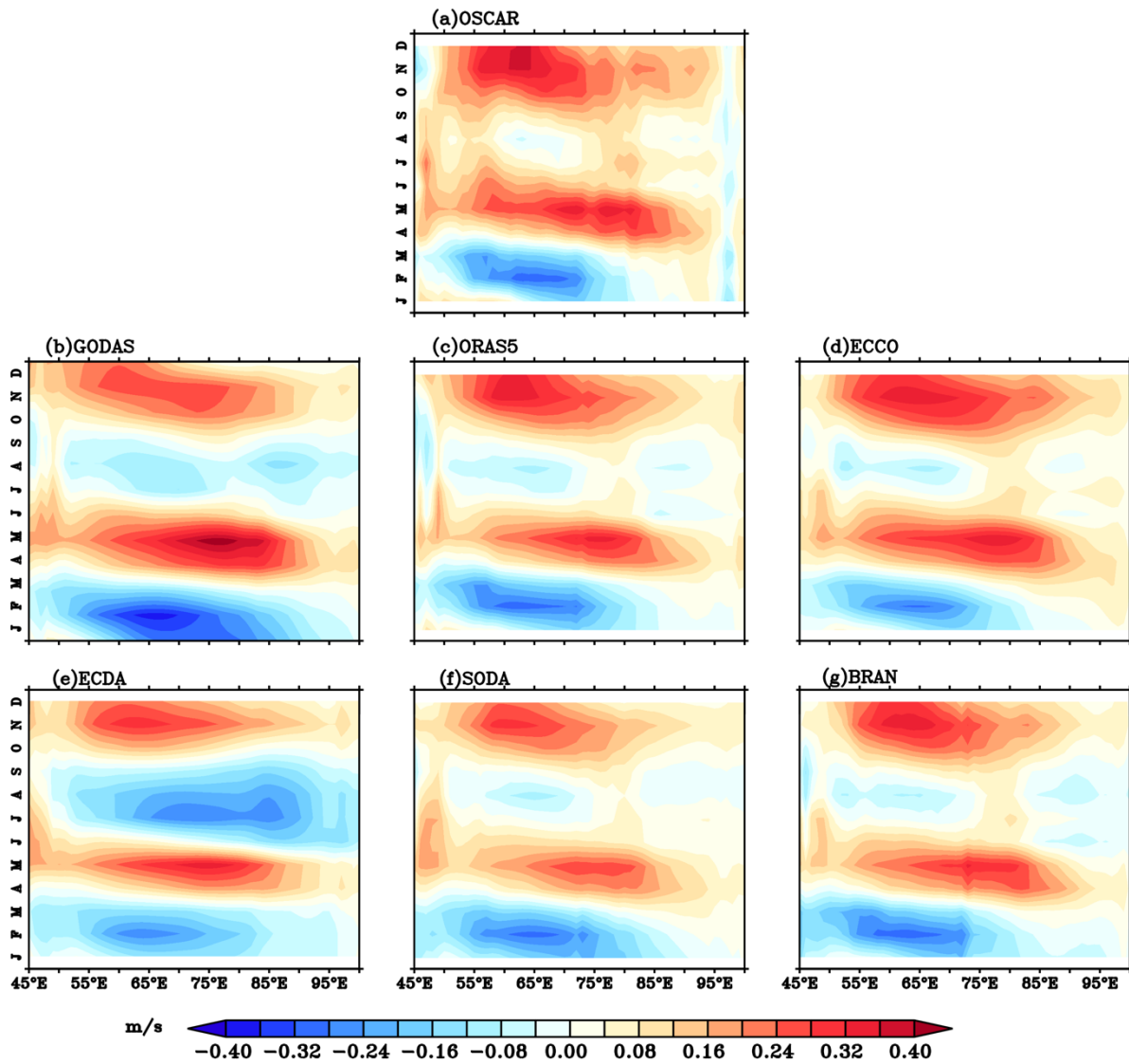


Fig. 4. Hovmoller diagram of monthly climatology of equatorial zonal currents (m/s) averaged over the region between 5°S and 5°N, extracted from (a) OSCAR, (b) GODAS, (c) ORAS5, (d) ECCO, (e) ECDA, (f) SODA, and (g) BRAN.

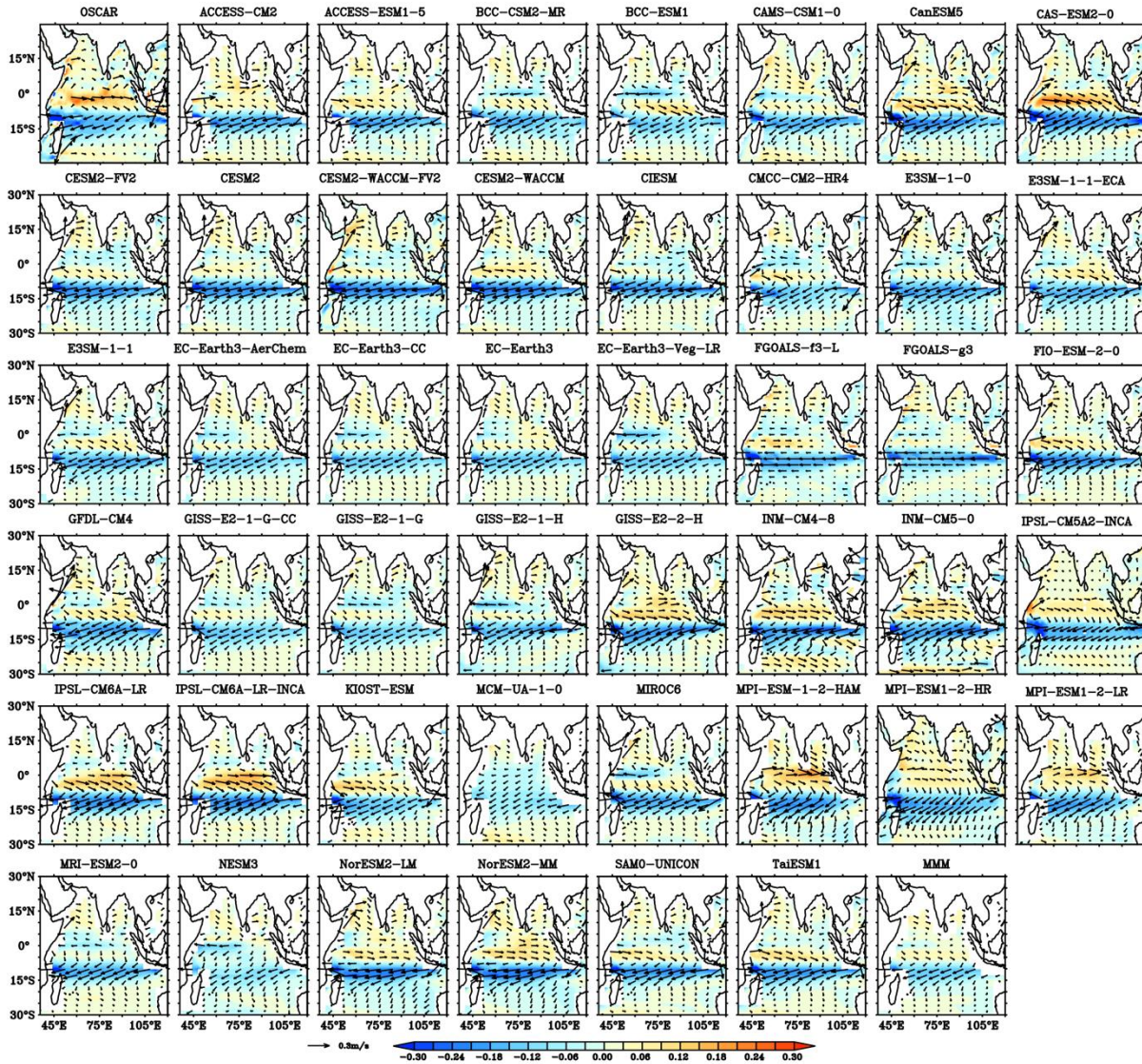


Fig. 5. The climatological mean of surface currents (m/s) from the OSCAR and the latest version of Coupled Model Intercomparison Project (CMIP6) 45 coupled models with their MMM.

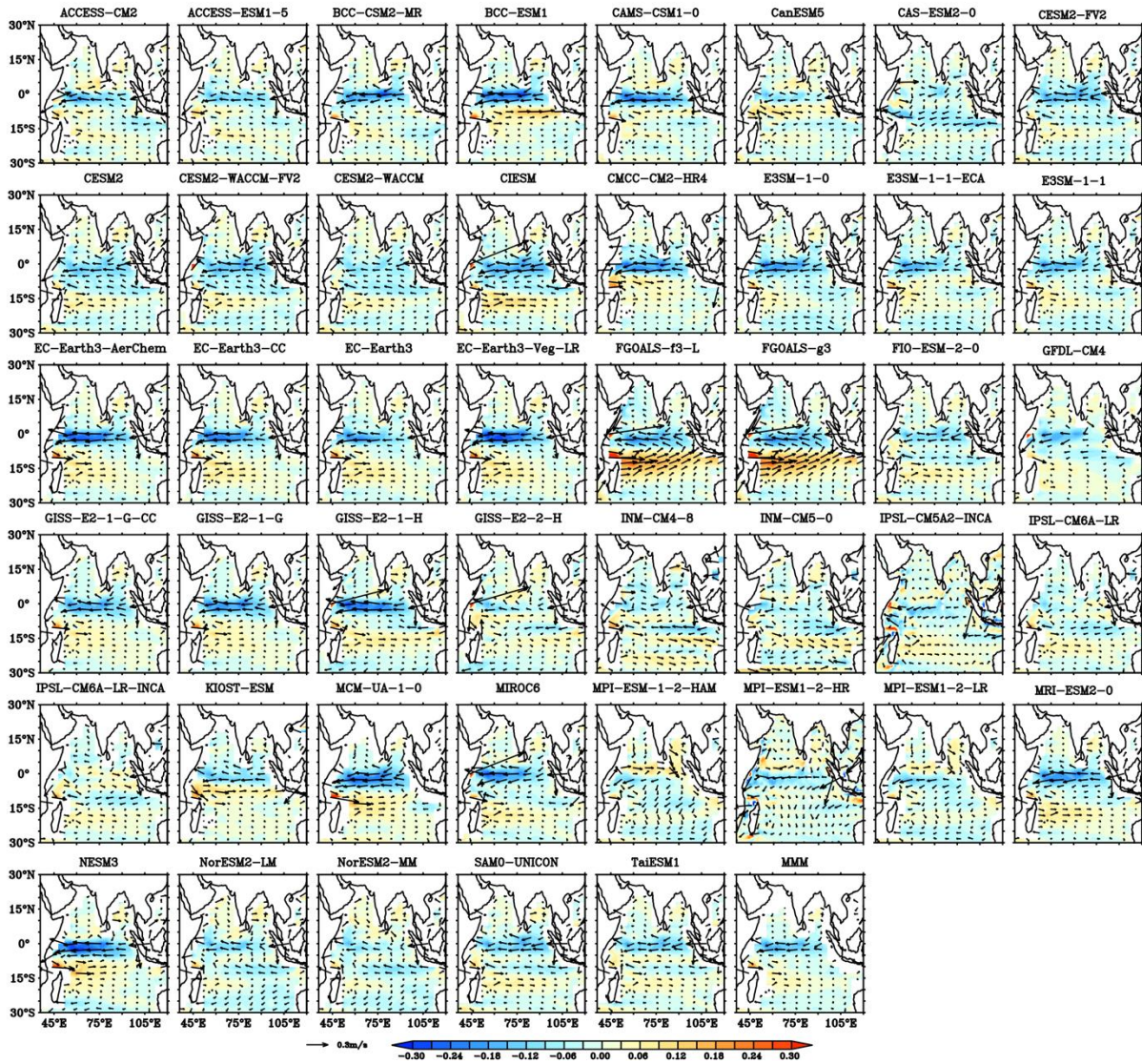


Fig. 6. Same as Figure 5 but for the surface currents bias (m/s). The bias is estimated as the difference between the model currents and OSCAR currents.

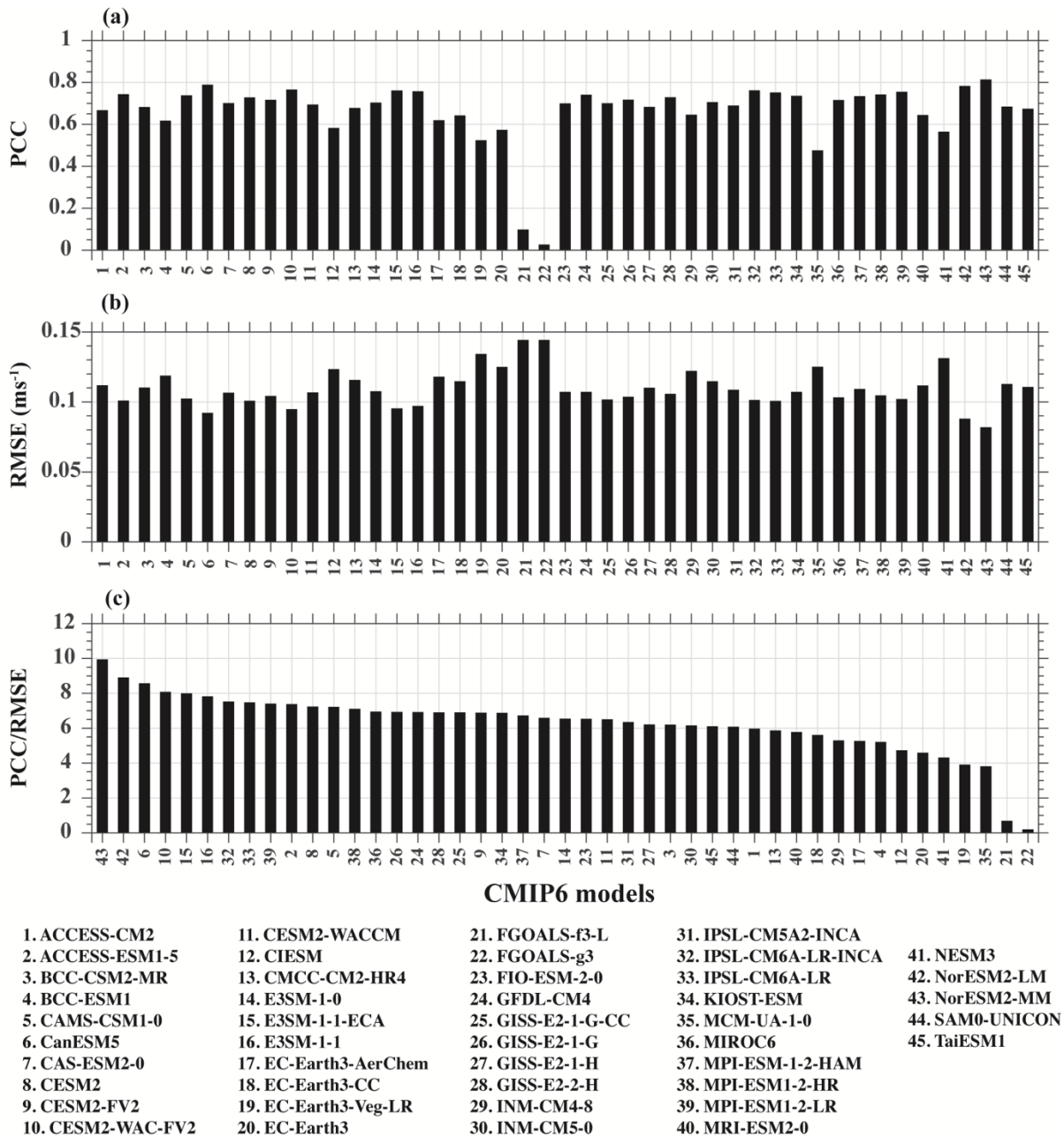


Fig. 7. Bar plots showing (a) PCC, (b) RMSE (m/s) for zonal currents simulated by CMIP6 with reference to OSCAR product. (c) The ratio of PCC to RMSE is used to rank the models and are sorted in descending order. Model names are given in the bottom panel.

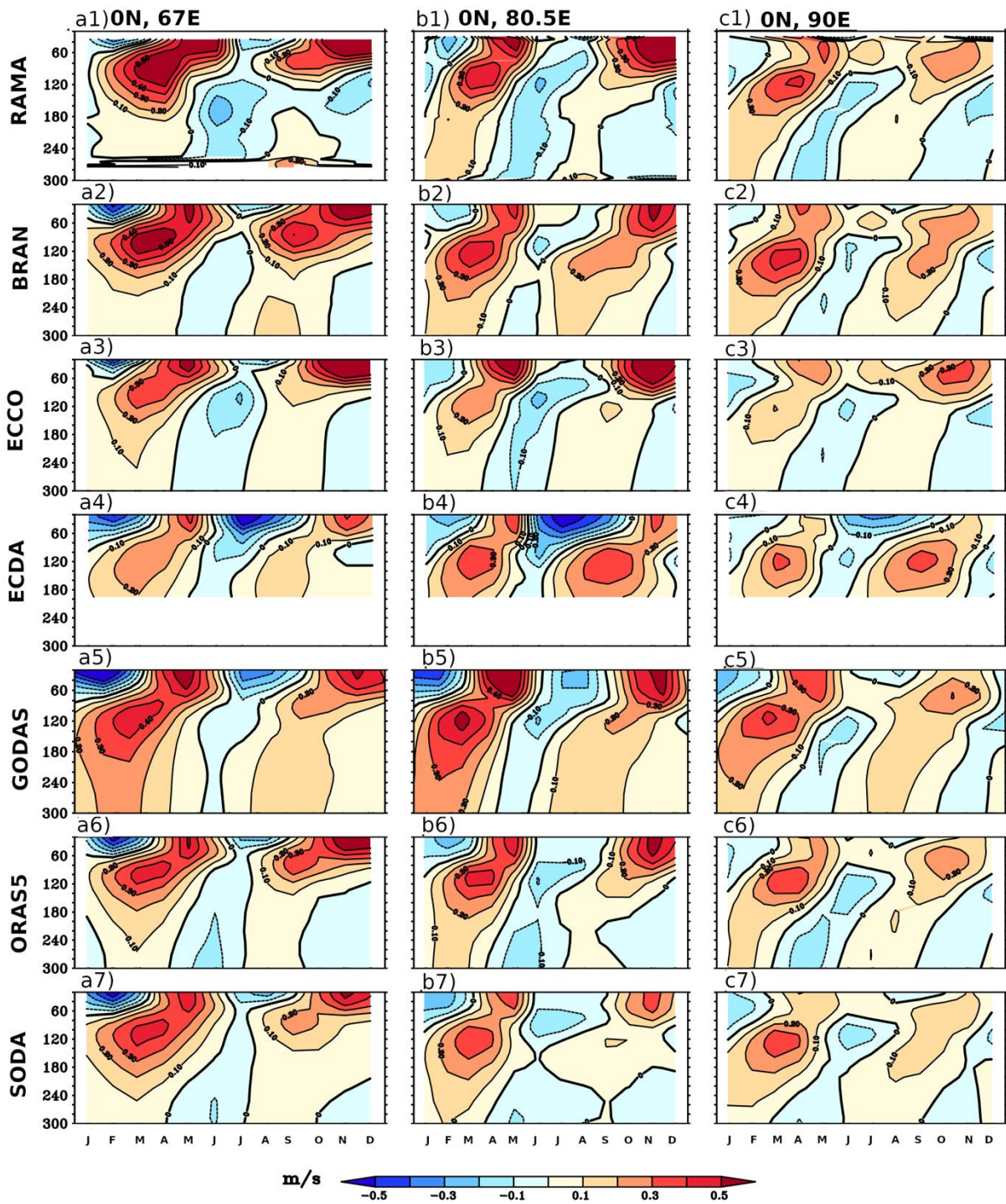


Fig. 8. The depth-time section of equatorial zonal currents (m/s) for mooring locations (a) 67°E, 0°N, (b) 90°E, 0°N, and (c) 80.5°E, 0°N from RAMA observations and reanalysis datasets BRAN, ECCO, ECDA, GODAS, ORAS5 and SODA respectively.

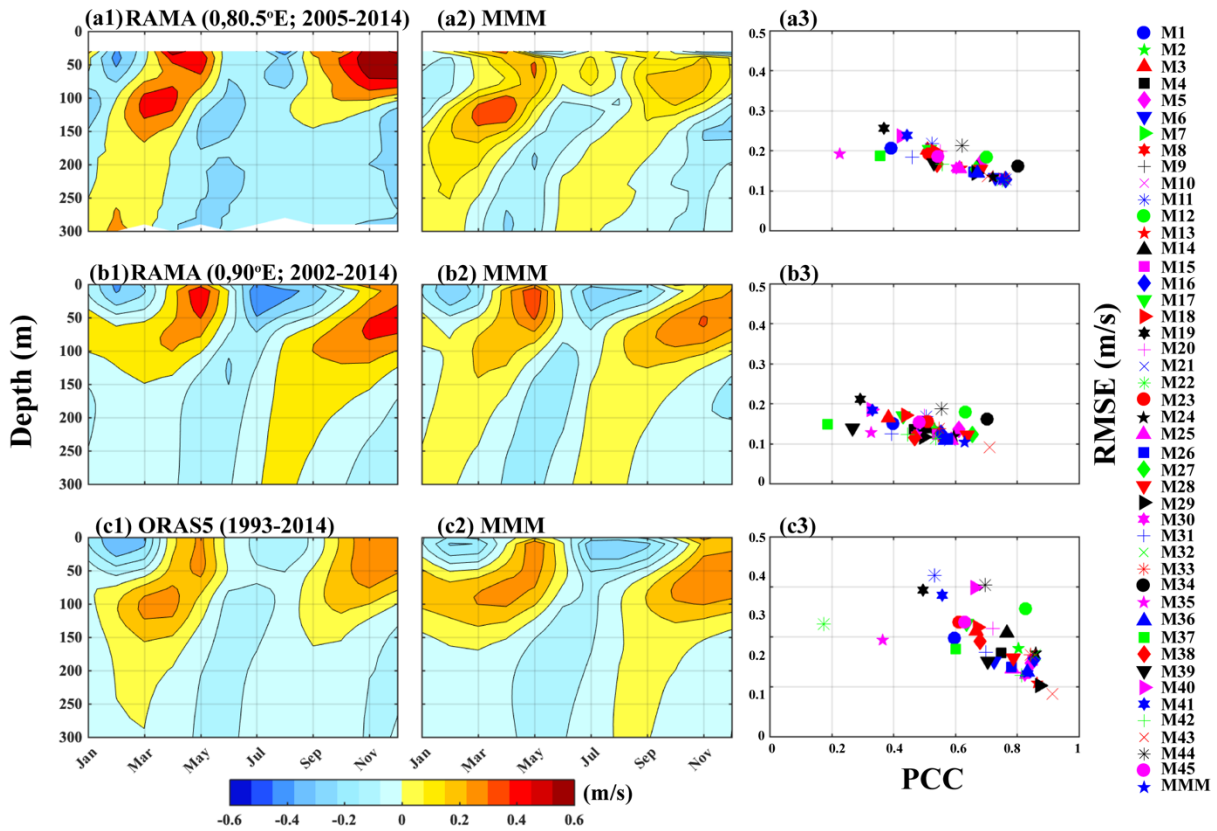


Fig. 9. Comparison of the seasonal cycle of zonal current structure from (a1-b1) RAMA buoys and the (a2-b2) multi-model mean (MMM) of CMIP6 historical simulations during their overlapping periods. (a3-b3) The intermodel scatterplot between the PCC and RMSE (m/s) for the seasonal climatology of zonal currents in individual CMIP6 models with respect to RAMA observations is also shown. (c1-c3) The climatological seasonal cycle at the equator (45°E-100°E) for the period 1993-2014 in ORAS5 and MMM are compared and corresponding PCC and RMSE values are shown for individual CMIP6 models.

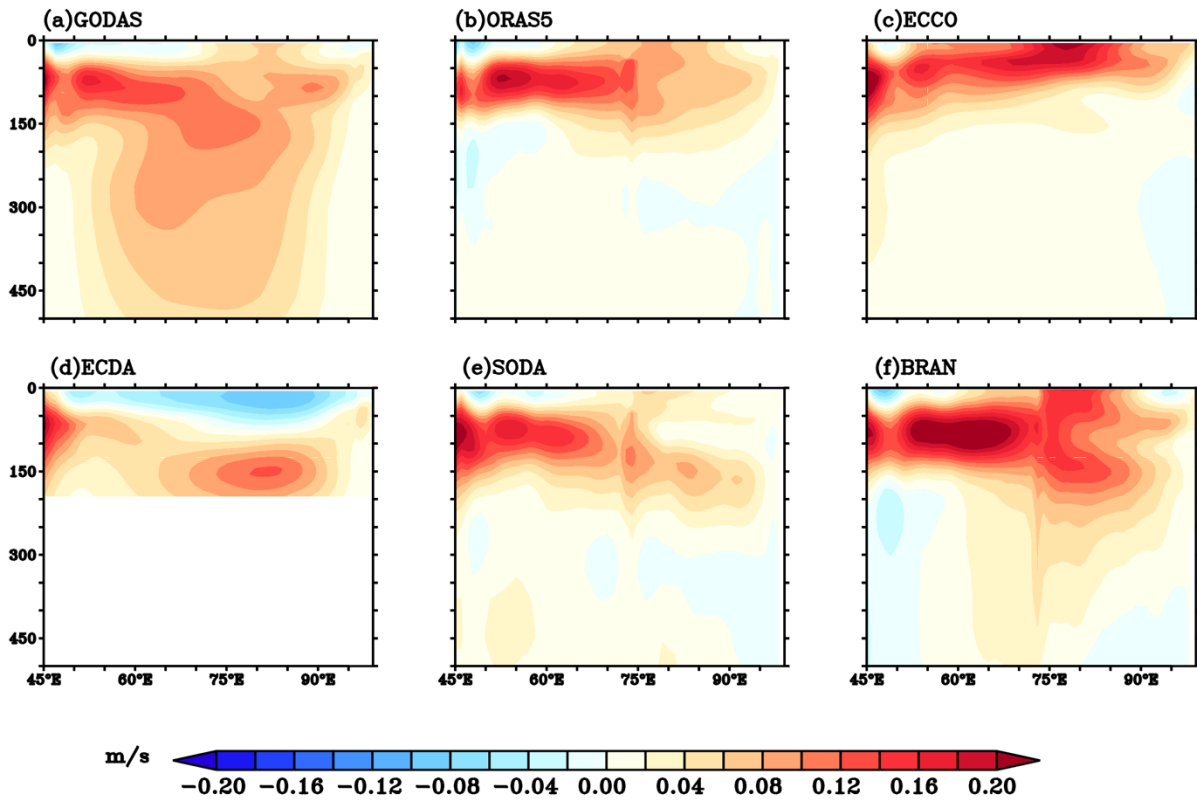


Fig. 10. The depth-longitude section of climatological zonal currents (m/s) in the upper 500m of equatorial Indian Ocean ($2^{\circ}\text{S} - 2^{\circ}\text{N}$) extracted from (a) GODAS, (b) ORAS5, (c) ECCO, (d) ECDA, (e) SODA, and (f) BRAN.

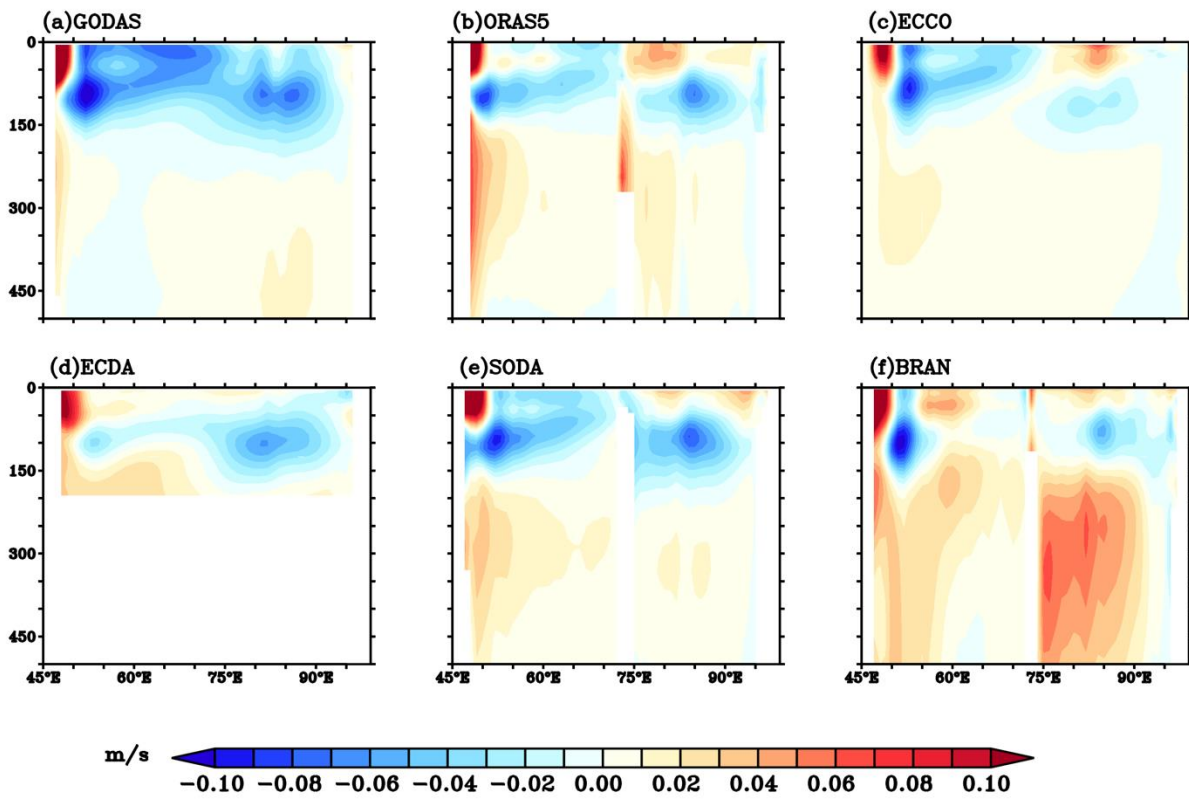


Fig.

11. Same as in Fig. 10, but the zonal currents (m/s) are averaged over north of equator (2° - 5° N).

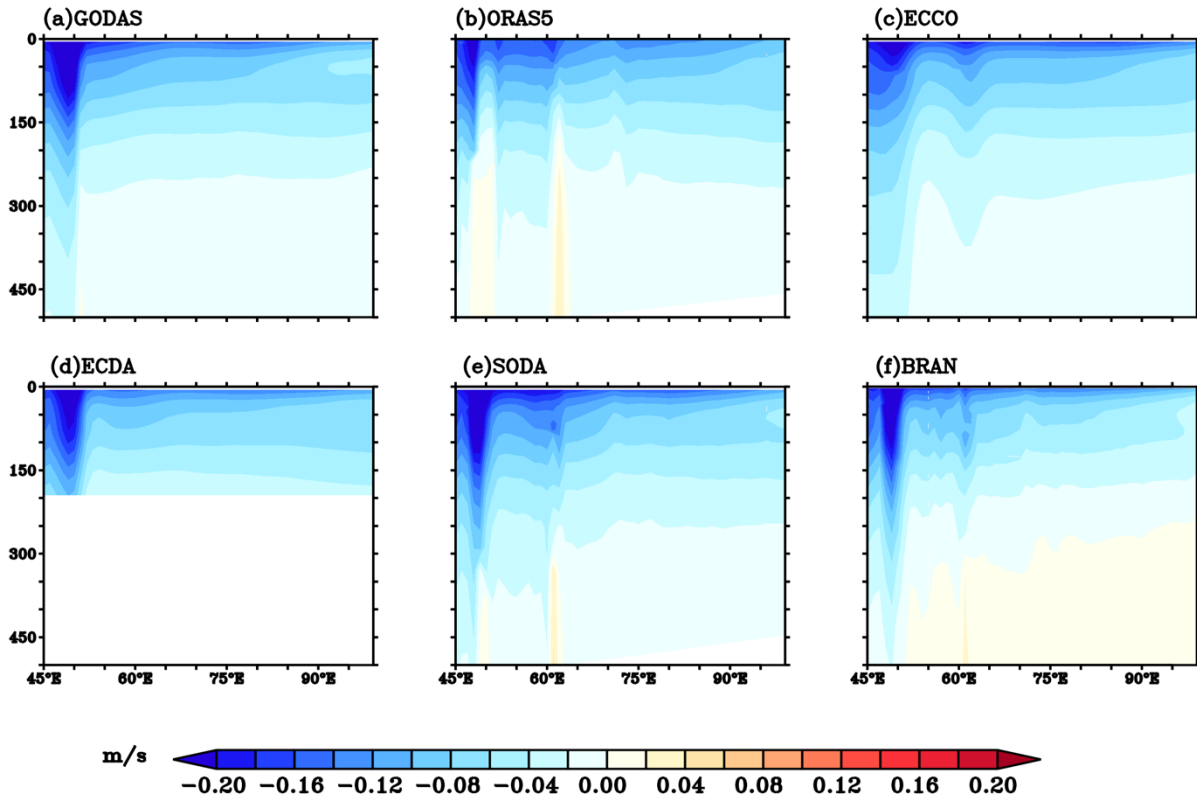


Fig. 12. Same as in Fig. 10, but the zonal currents (m/s) were averaged over south of the equator ($7^{\circ} - 15^{\circ}\text{S}$).

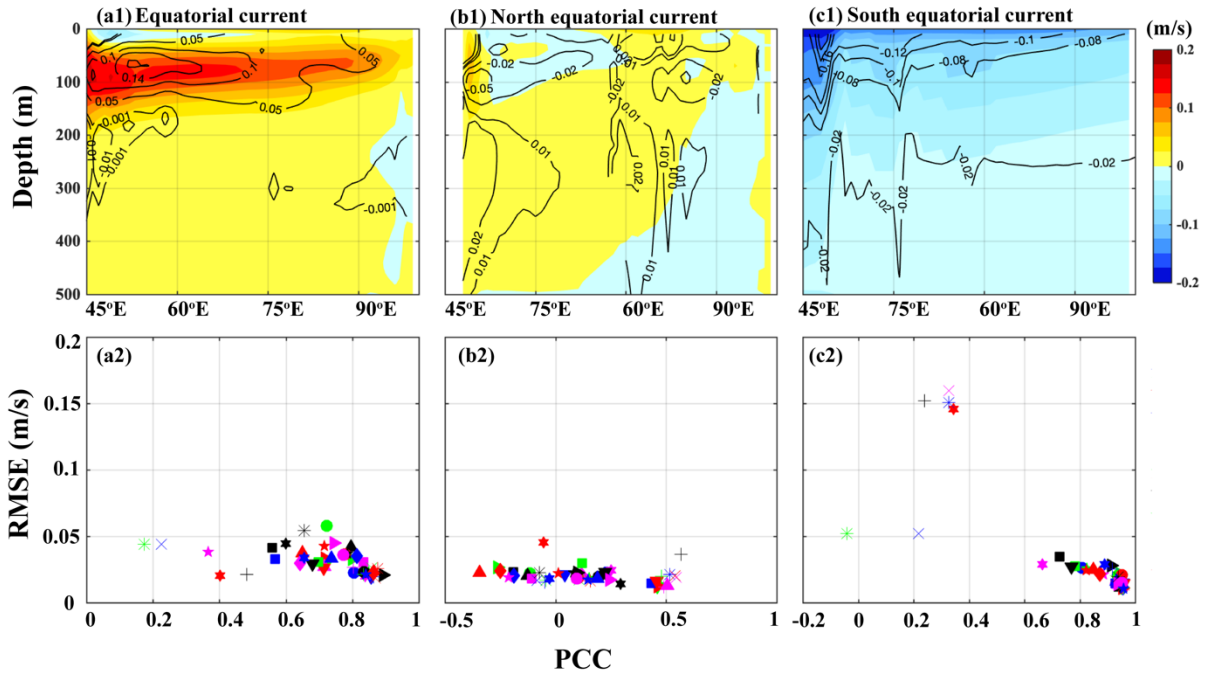


Fig. 13. Comparison of zonal current structure from (a1-c1) multi-model mean (MMM) of CMIP6 historical simulations during 1993-2014. Contours show the zonal current values (m/s) in ORAS5 for the respective current system. The inter-model scatterplot between the PCC and RMSE (m/s) for the zonal current structure in individual CMIP6 models compared with ORAS5. Model names are as in Figure 9.

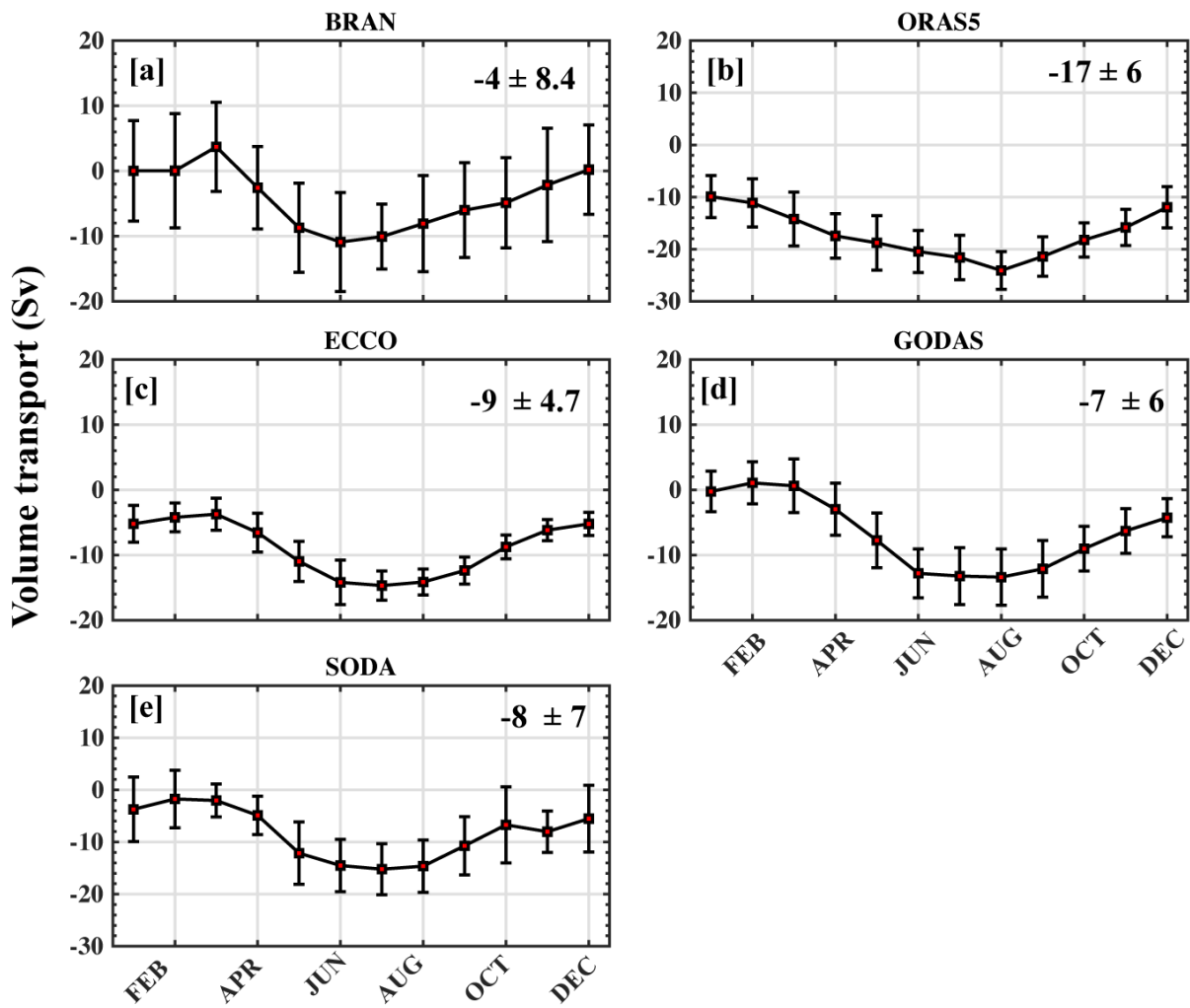


Fig. 14. Seasonal cycle of Indonesian Through Flow (ITF) volume transport in reanalysis products (a) – (e) BRAN, ORAS5, ECCO, GODAS and SODA respectively. Annual mean transport values in Sv are indicated on the top right side of the panels.

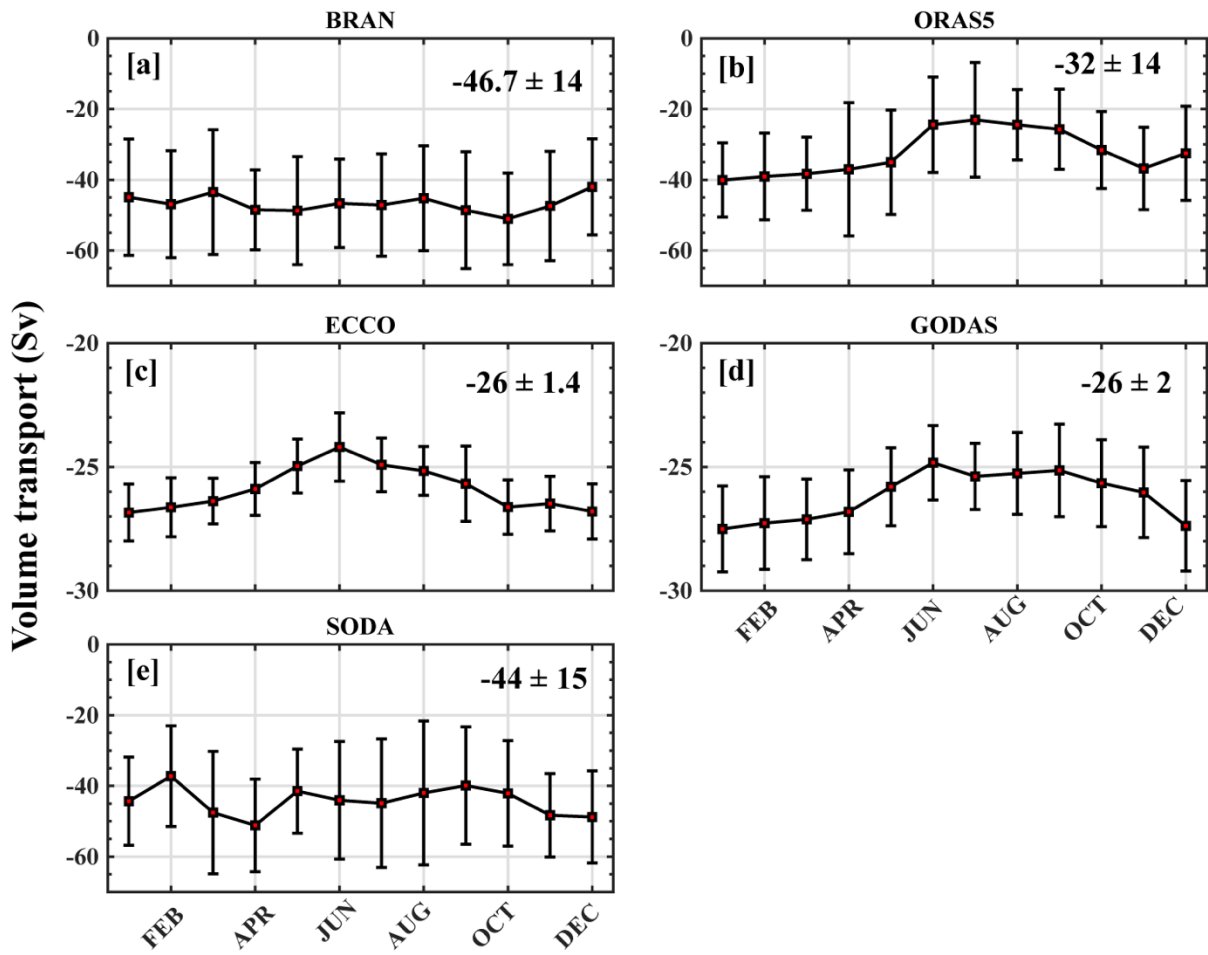


Fig. 15. Same as Figure 14 but for Agulhas leakage (AL).

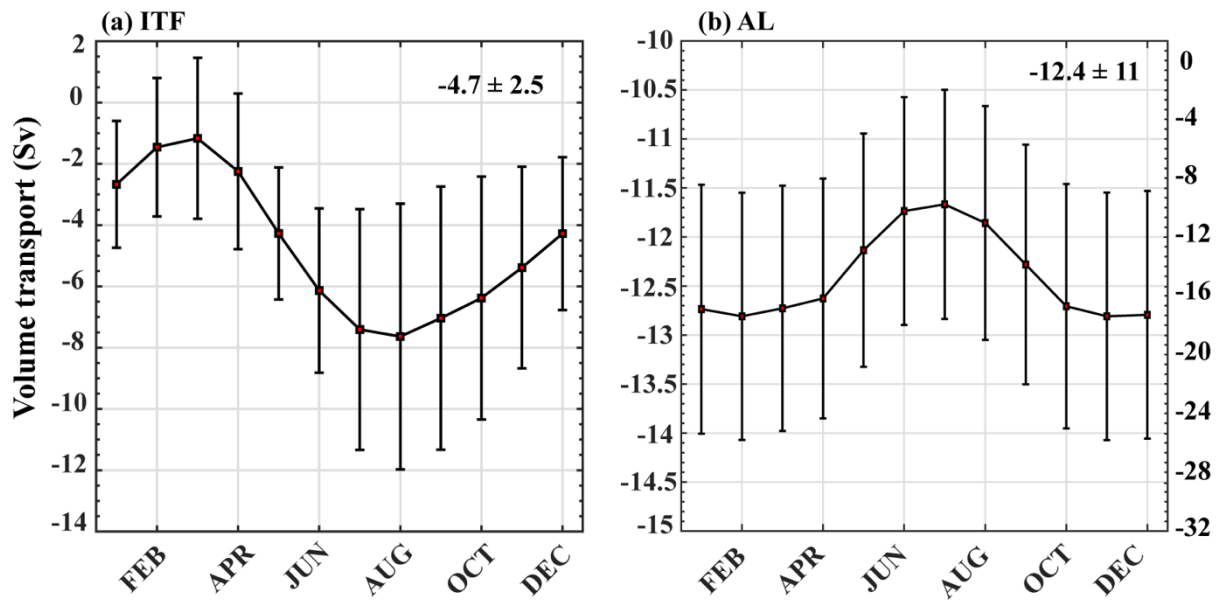


Fig. 16. Seasonal cycle of (a) Indonesian Through Flow (ITF) and (b) Agulhas leakage (AL) transports (m/s) from 45 CMIP6 models and their MMM with reference to ORAS5. Due to large inter-model spread and also to highlight the seasonal cycle, the upper and lower limits of error bars are referred to the right Y-axis in Figure 16b.

Tables:

Table 1. Details of RAMA buoys used in this study

Region	Location	Availability
EIO	0°E, 67°E	August 2014 - September 2019
	0°E, 80.5°E	November 2004 - July 2019
	0°E, 90°E	November 2001 - November 2017
SEIO	8.5°S, 106.75°E	January 2009 - May 2010

Table 2. Overview of six reanalysis datasets evaluated in this study

Dataset	GODAS	ORAS	ECCO	ECDA	SODA	BRAN
Version	-	S5	V4r3	V3.1	3.3.2	2020
Spatial resolution	1° meridional resolution is $\frac{1}{3}^\circ$ between 10°S and 10°N	1/4°	1/4°	1° x (0.3 -1°)	0.25° x 0.4°	1/10°
Atmospheric forcing	NCEP2 Reanalysis	ERA-Interim and ECMWF-NWP	ERA-Interim adjusted	Atmospheric component of the coupled model	JRA55	JRA55
Ocean component	MOM3	NEMO3.4.1 coupled to sea ice model	MITgcmLLC270	CM2.1	MOM5	OFAM3 MOM5
Vertical levels and first vertical level	40, 5	75, 0.5	50, 5	50, 5	50, 5	50, 2.5
Assimilated observations	Levitus climatology, Temperature profiles from XBT, moored buoys, Argo floats.	HadISST, AVISO SLA, Temperature and salinity profiles from EN4	In situ temperature salinity profiles from WOA09, AVHRR SST, CMEMS SLA, and GRACE	NCEP/NCAR reanalysis, T/S profiles from WOD09, NOAA OISST v2	AVHRR SST, In situ T/S profiles from WOD13	AVHRR SST, SLA from CMEMS, In situ T/S profiles
Reference	Behringer et al. (1998)	Zuo et al. (2019)	Forget et al. (2015)	Zhang et al. (2007)	Carton et al. (2018)	Chamberlain et al. (2021a,b)

Table 3. List of CMIP6 models considered in this study; their ocean component; vertical grid type (z: traditional height coordinate, z*: rescaled height coordinate for a more accurate representation of free surface variations, ρ : isopycnic, σ : terrain-following sigma coordinate, and multiple symbols represent hybrid coordinate system); resolution in latitude x longitude x number of vertical levels; and official reference.

Source:

https://www.ipcc.ch/report/ar6/wg1/downloads/report/IPCC_AR6_WGI_FOD_AnnexIII_Models.pdf

	CMIP6 model	Ocean component	Ocean vertical coordinate and levels	Nominal resolution of Oceanic component (lon x lat)	Reference
1	ACCESS-CM2	MOM5	z*, 50	1° x 0.6°	Bi et al. (2020)
2	ACCESS-ESM1-5	MOM5	z*, 50	1° x 0.6°	Ziehn et al. (2020)
3	BCC-CSM2-MR	MOM4-140	z, 40	1° x 0.78°	Wu et al. (2019)
4	BCC-ESM1	MOM4	z, 40	1° x 0.78°	Wu et al. (2019)
5	CAMS-CSM1-0	MOM4	z, 50	1° x 0.9°	Rong et al. (2019)
6	CanESM5	NEMO3.4.1	z, 45	1° x 0.6°	Swart et al. (2019)
7	CAS-ESM2-0	LICOM2.0	z, 30	1° x 0.9°	Guangqing et al. (2020)

8	CESM2	POP2	z, 60	1.125° x 0.5°	Danabasoglu et al. (2020)
9	CESM2-FV2	POP2	z, 60	1.125° x 0.5°	Danabasoglu (2019b)
10	CESM2-WACCM-FV2	POP2	z, 60	1.125° x 0.5°	Danabasoglu (2019b)
11	CESM2-WACCM	POP2	z, 60	1.125° x 0.5°	Danabasoglu (2019)
12	CIESM	CIESM-OM	z, 46	0.5° x 0.32°	Lin et al. 2020
13	CMCC-CM2-HR4	NEMO3.6	z, 50	0.25° x 0.25°	Scoccimarro (2019)
14	E3SM-1-0	MPAS-Ocean	z*, 60	1° x 1°	Golaz et al. (2019)
15	E3SM-1-1-ECA	MPAS-Ocean	z, 60	1° x 1°	Burrows et al. (2019)
16	E3SM-1-1	MPAS-Ocean	z, 60	1° x 1°	Burrows et al. (2019)
17	EC-Earth3-AerChem	NEMO3.6	z, 75	1° x 0.6°	van Noije et al. (2021)
18	EC-Earth3-CC	NEMO3.6	z, 75	1° x 0.6°	Döscher et al. (2021)

19	EC-Earth3-Veg-LR	NEMO3.6	z, 75	1° x 0.6°	EC-Earth (2020)
20	EC-Earth3	NEMO3.6	z, 75	1° x 0.6°	EC-Earth (2019a)
21	FGOALS-f3-L	LICOM3.0	z, 30	1° x 0.8°	He et al. (2019)
22	FGOALS-g3	LICOM3.0	z, 30	1° x 0.8°	Li et al. (2020)
23	FIO-ESM-2-0	POP2-W	z, 60	1.125° x 0.5°	Bao et al. (2020)
24	GFDL-CM4	MOM6	$\rho - z^*$, 75	0.25° x 0.25°	Guo et al. (2018)
25	GISS-E2-1-G-CC	GISS Ocean	z, 40	1° x 1°	Miller et al. (2021)
26	GISS-E2-1-G	GISS Ocean	z, 40	1° x 1°	Kelley et al. (2020)
27	GISS-E2-1-H	HYCOM	z - ρ - σ , 32	1° x 1°	NASA/GISS et al. (2018)
28	GISS-E2-2-H	GISS Ocean	z, 40	1° x 1°	
29	INM-CM4-8	INM-OM5	σ , 40	1° x 0.56°	Volodin et al. (2013)
30	INM-CM5-0	INM-OM5	σ , 40	0.5° x 0.25°	Volodin et al. (2017)

31	IPSL-CM5A2-INCA	NEMO-OPA	z, 31	2° x 1.2°	Sepulchre et al. (2020)
32	IPSL-CM6A-LR-INCA	NEMO-OPA	z, 31	1° x 0.54°	Boucher et al. (2020)
33	IPSL-CM6A-LR	NEMO3.6	z*, 31	1° x 0.54°	Boucher et al. (2020)
34	KIOST-ESM	MOM5	z*, 52	1° x 0.9°	Pak et al. (2021)
35	MCM-UA-1-0	MOM1	z, 18	2° x 2°	Delworth et al. (2002)
36	MIROC6	COCO4.9	z-σ, 63	1° x 0.7°	Shiogama et al. (2020)
37	MPI-ESM-1-2-HAM	MPIOM1.6.3	z, 40	1.5° x 0.8°	Mauritsen et al. (2019)
38	MPI-ESM1-2-HR	MPIOM1.6.3	z, 40	0.5° x 0.4°	Gutjahr et al. (2019)
39	MPI-ESM1-2-LR	MPIOM1.6.3	z, 40	1.4° x 0.82°	Gutjahr et al. (2019)
40	MRI-ESM2-0	MRI.COM4.4	z*, 61	1° x 0.5°	Yukimoto et al. (2019)

41	NESM3	NEMO3.4	z, 46	1° x 0.5°	Cao et al. (2018)
42	NorESM2-LM	MICOM	z - ρ, 70	1° x 1°	Seland et al. (2020)
43	NorESM2-MM	MICOM	z - ρ, 70	1° x 1°	Seland et al. (2020)
44	SAM0-UNICON	POP2	z, 60	1.125° x 0.5°	Park et al. (2019)
45	TaiESM1	POP2	z, 60	1.125° x 0.5°	Lee, Wang, et al. (2021)

Table 4. The PCC of spring and fall climatology of Wyrтки jets in reanalysis against OSCAR

Sl No.	Product	Spring (MAM)	Fall (SON)
1	BRAN	0.91	0.97
2	ECCO	0.82	0.96
3	ECDA	0.41	0.6
4	GODAS	0.65	0.76
5	ORAS5	0.84	0.94
6	SODA	0.78	0.91

Table 5. PCC and RMSE values of monthly mean values of reanalysis products at RAMA buoy locations during their overlapping period. Depth considered is from surface to 300m.

		PCC				RMSE			
		0°E, 67°E (2015- 2017)	0°E, 80.5°E (2005- 2017)	0°E, 90°E (2002- 2016)	8.5°S, 106.75°E (2009)	0°E, 67°E (2015- 2017)	0°E, 80.5°E (2005- 2017)	0°E, 90°E (2002- 2016)	8.5°S, 106.75°E (2009)
1	GODAS	0.65	0.81	0.77	0.81	0.17	0.14	0.11	0.12
2	ORAS5	0.75	0.93	0.9	0.41	0.15	0.07	0.06	0.18
3	ECCO	0.82	0.92	0.8	0.63	0.14	0.08	0.08	0.15
4	ECDA	0.32	0.55	0.52	0.37	0.24	0.2	0.16	0.24
5	SODA	0.66	0.83	0.81	0.62	0.18	0.12	0.082	0.15
6	BRAN	0.66	0.88	0.81	0.91	0.24	0.12	0.092	0.08